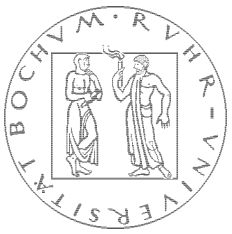

Ruhr University Bochum
Lehrstuhl für Technische Mechanik

Preprint 01-2005

Numerical analyses of discontinuous material bifurcation: Strong and weak discontinuities

J. Mosler

This is a preprint of an article published in:

Computer Methods in Applied Mechanics and Engineering, Vol. 194, Issues 9–11, 979–100, (2005)

Numerical analyses of discontinuous material bifurcation: Strong and weak discontinuities

J. Mosler

Lehrstuhl für Technische Mechanik
Ruhr University Bochum
Universitätsstr. 150,D-44780 Bochum, Germany
E-Mail: mosler@tm.bi.ruhr-uni-bochum.de
URL: www.tm.bi.ruhr-uni-bochum.de/mosler

SUMMARY

In this paper an algorithmic formulation for numerical analyses of material bifurcation is presented. Conditions for the onset of both weak discontinuities (discontinuous strain rates) and strong discontinuities (discontinuous velocity fields) are summarized. Based on a recently proposed plasticity model formulated within the logarithmic strain space, the condition for the formation of strong discontinuities is extended to anisotropic finite strain plasticity theory. The resulting equations associated with the mode of bifurcation are solved numerically. For that purpose, an equivalent optimization problem is considered. The algorithmic formulation is based on NEWTON's method using a consistent linearization. To enlarge the radius of convergence, a line search strategy is applied. The applicability of the proposed implementation as well as its performance and numerical robustness is investigated by means of three-dimensional numerical bifurcation analyses of a DRUCKER-PRAGER type plasticity model.

1 INTRODUCTION

For a better understanding of the mechanical behavior of materials, the knowledge about their corresponding failure modes is of utmost importance. For instance, the mode I failure associated with concrete subjected to tensile loading leads to a sudden drop in the residual strength of the material. In contrast to this, shear bands and slip lines (mode II failure) typically appear in metals and in saturated soils. In general, these mechanisms show a more ductile material response.

From a macroscopic point of view, material failure is often accompanied by the formation of narrow zones with high gradients of the displacement field. For impressive illustrations of such localized deformation fields, we refer to [1]. In the limit case, the gradient of the displacement field (GRAD$\boldsymbol{u}$) is discontinuous (weak discontinuity). The condition for the transition from homogeneously distributed deformations (see Fig. 1a) to discontinuous strain fields (see Fig. 1b) has been implicitly developed by HADAMARD [2]. HADAMARD analyzed the dispersion of waves in solids and derived the condition for real valued wave speeds. Not until the 70's the connection between HADAMARD's work and the transition from homogeneously distributed deformations to localized failure was understood. RUDNICKI & RICE [3] [4] studied this transition for different materials and computed the corresponding bifurcation modes. RANIECKI & BRUHNS [5] extended the ideas of RUDNICKI & RICE to non-associated finite strain plasticity. For the geometrically linear theory explicit formulas for different plasticity based continuum

models have been proposed in [6, 7]. The counterparts for damage mechanics have been given in [8].

If the width of the zones exhibiting localized deformations converges to zero (see Fig. 1), a discontinuity in the displacement field forms. This limit case is often denoted as strong discontinuity. The conditions for the onset of discontinuous displacement fields have been analyzed by SIMO, OLIVER & ARMERO [9]. Before bifurcation, SIMO, OLIVER & ARMERO assumed a homogeneously distributed deformation field. The extension to finite strain plasticity was proposed in [10]. In contrast to [9, 10], OLIVER studied the transition from weak to strong discontinuities [11]. On the basis of an evolution law for the width of the zone in which localized deformations appear, the connection between both types of material bifurcation was achieved. The corresponding extension to finite strains was presented in [12]. However, both finite strain models [10, 12] are based on a space of admissible stresses formulated in terms of KIRCHHOFF stresses together with an isotropic softening evolution (and without structural tensors). Consequently, they are restricted to isotropic yield surfaces. In this paper, we extend the ideas proposed in [10] to anisotropic finite strain plasticity theory.

The conditions associated with the formation of weak and strong discontinuities result in sets of equations formally identical to each other (see [10]). However, closed form solutions are not available for more complicated material models. Hence, the development of numerical procedures is of utmost importance. To the best knowledge of the author, these algorithmic formulations have been primarily suggested by ORTIZ [13, 14]. In these references, implementations were proposed for both two-dimensional as well as three-dimensional problems. Despite the efficiency of these numerical models, some modifications and extensions are necessary. On the one hand ORTIZ's derivations hold only for symmetrical acoustic tensors. This implies an associative flow rule. On the other hand the iterative algorithmic formulation as suggested in [13, 14] is based on a generalized eigenvalue problem. In contrast to this procedure, a NEWTON-type iteration scheme is applied. By using a parameterization of the normal vector of the surface of strong or weak discontinuities in terms of spherical coordinates, an efficient numerical model characterized by an asymptotic quadratic rate is developed. To enlarge the radius of convergence, the proposed implementation is improved by means of a line search strategy.

In general, the solution of the localization conditions is not unique. Consequently, it is necessary to chose the „right" solution from the set of all candidates. For that purpose, different strategies are analyzed critically. The analogies between them are pointed out.

The paper is organized as follows: Section 2 is concerned with an introduction to singular surfaces. In particular, a mathematically consistent definition of these surfaces is proposed. In Section 3, a concise review of the localization condition associated with the formation of weak discontinuities is given. The localization condition associated with the formation of strong discontinuities is discussed in Section 4. On the basis of a finite strain plasticity model recently proposed in [15, 16], the conditions for the onset of strong discontinuities are extended to anisotropic materials. The algorithmic formulation of both bifurcation conditions is proposed in Section 5. The applicability of the implementation as well as its performance and numerical robustness is investigated in Section 6. In Section 7, different strategies are presented to chose the „right" solution from the set of all candidates. Each concept is analyzed critically.

2 SINGULAR SURFACES

This section is concerned with a mathematical classification of weak and strong discontinuities (see [17]). For that purpose, it is convenient to introduce the definition of a singular surface $\partial_s\Omega$ (see Fig. 1).

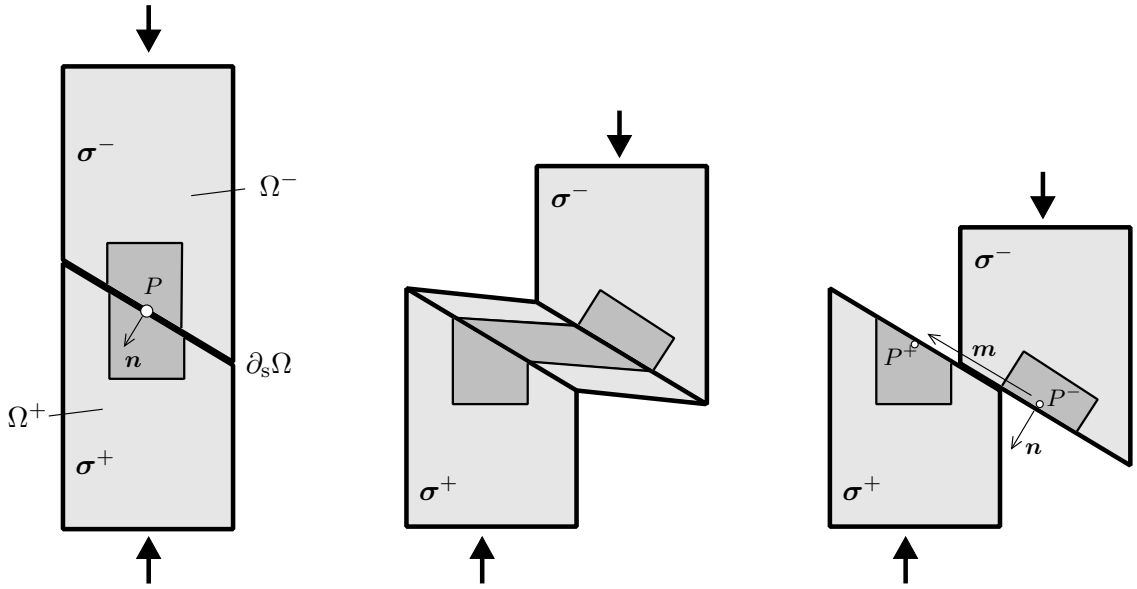

$\dot{\boldsymbol{u}}^+ = \dot{\boldsymbol{u}}^-$	$\dot{\boldsymbol{u}}^+ = \dot{\boldsymbol{u}}^-$	$\dot{\boldsymbol{u}}^+ \neq \dot{\boldsymbol{u}}^-$
$\mathrm{GRAD}\dot{\boldsymbol{u}}^+ = \mathrm{GRAD}\dot{\boldsymbol{u}}^-$	$\mathrm{GRAD}\dot{\boldsymbol{u}}^+ \neq \mathrm{GRAD}\dot{\boldsymbol{u}}^-$	$\mathrm{GRAD}\dot{\boldsymbol{u}}^+ \neq \mathrm{GRAD}\dot{\boldsymbol{u}}^-$
a) homogeneous	b) weak discontinuity	c) strong discontinuity

Figure 1: Different stages of the formation of a shear band observed in soils (uniaxial compression test).

From a mathematical point of view, the domain $\partial_\mathrm{s}\Omega$ represents a two-dimensional submanifold in $\mathbb{R}^3$. This hyperplane is characterized by a chart $\boldsymbol{\Upsilon} : \mathbb{R}^2 \supseteq \mathcal{U} \rightarrow \mathcal{M} \subseteq \partial_\mathrm{s}\Omega$. For further derivations, it is sufficient to postulate $\boldsymbol{\Upsilon} \in \mathrm{Diff}^1(\mathcal{U},\mathcal{M}) \supset \mathrm{Diff}^\infty(\mathcal{U},\mathcal{M})$. These conditions imply, that $\boldsymbol{\Upsilon}$ is a one-to-one mapping ($\boldsymbol{\Upsilon} \in \mathrm{Diff}^1(\mathcal{U},\mathcal{M}) \Rightarrow \exists!\ \boldsymbol{\Upsilon}^{-1} \in \mathrm{Diff}^1(\mathcal{M},\mathcal{U})$: $\boldsymbol{\Upsilon}^{-1} \circ \boldsymbol{\Upsilon} = \boldsymbol{id}_\mathcal{U}$) and the normal vector $\boldsymbol{N} \in N_{X_0}$ of the surface $\partial_\mathrm{s}\Omega$ at the position $\boldsymbol{X}_0 \in \mathcal{M}$ is well defined ($\boldsymbol{\Upsilon} \in C^1(\mathcal{U},\mathcal{M}) \ \Rightarrow\ \dim N_{X_0} = 1$). In the context of material bifurcation, a hyperplane $\partial_\mathrm{s}\Omega$ with the described properties represents a singular surface with respect to a given mapping $\boldsymbol{\varphi} : \bar{\Omega} \rightarrow \mathbb{R}^3$ if the additional condition

$$\forall \boldsymbol{X}_0 \in \partial_\mathrm{s}\Omega,\ \forall \varepsilon > 0,\ \ \boldsymbol{\varphi}|_{B\,(\boldsymbol{X}_0,\varepsilon)} \notin \mathcal{C}^\infty, \tag{1}$$

with

$$B(\boldsymbol{X}_0,\varepsilon) := \{\boldsymbol{X} \in \Omega \mid\ ||\boldsymbol{X}_0 - \boldsymbol{X}||_2 < \varepsilon\} \tag{2}$$

holds. Consequently, the order of a singular surface

$$p := \inf\left\{ c \in \mathbb{N}_0 \ \middle|\ \frac{\partial^c \boldsymbol{\varphi}(\boldsymbol{X})}{\partial \boldsymbol{X}^c} \notin C^0\left(\Omega,\ \mathbb{R}^{3^{a+1}}\right) \right\} \tag{3}$$

is well defined. According to Eq. (3), the order of a singular surface indicates the lowest order derivative exhibiting a discontinuity. Focusing our considerations to nonlinear continuum mechanics (LAGRANGE description), the function $\boldsymbol{\varphi}$ is represented by the deformation mapping. Hence, zero-order singular surfaces are associated with a discontinuity of the deformation map and the displacement field (strong discontinuities), respectively. First-order singular surfaces are characterized by a jump in the field of the deformation gradient (weak discontinuities).

For further derivations, we introduce the notation

$$\boldsymbol{g} := \frac{\partial^p \boldsymbol{\varphi}(\boldsymbol{X})}{\partial \boldsymbol{X}^p} \notin C^0\left(\Omega,\ \mathbb{R}^{3^{a+1}}\right). \tag{4}$$

Consequently, without loss of generality, the following derivations can be restricted to zero-order singular surfaces. Introducing the oscillation of a function $\boldsymbol{g}$ in $\boldsymbol{X}_0 \in \Omega$

$$\omega_{\boldsymbol{g}}(\boldsymbol{X}_0) := \inf_{\delta>0} \sup_{\boldsymbol{X}_1,\, \boldsymbol{X}_2 \in B(\boldsymbol{X}_0,\delta)} ||\boldsymbol{g}(\boldsymbol{X}_1) - \boldsymbol{g}(\boldsymbol{X}_2)||_2 \,, \tag{5}$$

the topology of $\partial_{\mathrm{s}}\Omega$ is obtained as

$$\partial_{\mathrm{s}}\Omega := \{\boldsymbol{X} \in \Omega \mid \omega_{\boldsymbol{g}}(\boldsymbol{X}) \neq 0\}. \tag{6}$$

For a planar surface $\partial_{\mathrm{s}}\Omega$ [9, 18–20] defined by its normal $\boldsymbol{N}$, the sets Ω^- and Ω^+ (see Fig. 1) result in

$$\begin{aligned} \Omega^+ &:= \left\{\boldsymbol{X} \in \Omega \mid (\boldsymbol{X}-\boldsymbol{A})\cdot\boldsymbol{N}|_{\boldsymbol{A}} > 0\right\} \\ \Omega^- &:= \left\{\boldsymbol{X} \in \Omega \mid (\boldsymbol{X}-\boldsymbol{A})\cdot\boldsymbol{N}|_{\boldsymbol{A}} < 0\right\} \end{aligned} \qquad \boldsymbol{A} \in \partial_{\mathrm{s}}\Omega. \tag{7}$$

On the basis of Eqs. (7), it can be easily checked if a given point belongs to Ω^- or Ω^+, respectively. Hence, the format (7) is well suitable for finite element formulations characterized by discontinuous displacement fields [17].

Restricting the mapping $\boldsymbol{g}$ to piecewise continuous functions ($\boldsymbol{g} \in S(\Omega,\ \mathbb{R}^{3^{a+1}})$), the left-hand and the right-hand limits are well defined

$$\begin{aligned} \boldsymbol{g}^+(\boldsymbol{A}) &:= \lim_{\boldsymbol{X}\in\Omega^+\to\boldsymbol{A}} \boldsymbol{g} \\ \boldsymbol{g}^-(\boldsymbol{A}) &:= \lim_{\boldsymbol{X}\in\Omega^-\to\boldsymbol{A}} \boldsymbol{g}, \end{aligned} \qquad \boldsymbol{A} \in \partial_{\mathrm{s}}\Omega \tag{8}$$

and the discontinuity of $\boldsymbol{g}$ in $\boldsymbol{A}$ is obtained as

$$[\![\boldsymbol{g}(\boldsymbol{A})]\!] := \boldsymbol{g}^+(\boldsymbol{A}) - \boldsymbol{g}^-(\boldsymbol{A}). \tag{9}$$

By comparison of Eq. (9) and (5), the identity

$$\omega_{\boldsymbol{g}}(\boldsymbol{A}) = ||\,[\![\boldsymbol{g}(\boldsymbol{A})]\!]\,||_2 \tag{10}$$

follows. Consequently, the oscillation is equivalent to the amplitude of the discontinuity.

In the following paragraph, the compatibility conditions associated with a singular surface of degree p are summarized. For that purpose, it is convenient to formulate these conditions in terms of the displacement field $\boldsymbol{u}$. From the LAGRANGE description of deformation

$$\begin{aligned} \boldsymbol{\varphi}:\ \bar{\Omega} &\to \mathbb{R}^3 \\ \boldsymbol{X} &\mapsto \boldsymbol{x} := \boldsymbol{X} + \boldsymbol{u} \end{aligned} \tag{11}$$

and the assumption of continuity of the reference placement ($[\![\boldsymbol{X}]\!] = \boldsymbol{0}$), the compatibility condition of a zero-oder singular surface reads

$$[\![\boldsymbol{x}]\!] = [\![\boldsymbol{u}]\!] =: \zeta\, \boldsymbol{m}, \quad \text{with} \quad ||\boldsymbol{m}||_2 = 1, \quad \zeta = \omega_{\boldsymbol{u}}. \tag{12}$$

Condition (12) connects the displacement field in Ω^- and Ω^+. According to Eq. (10), ζ represents the amplitude of the displacement discontinuity and $\boldsymbol{m}$ denotes the corresponding direction vector. Based on Eqs. (12), the compatibility conditions for higher order singular surfaces can be derived successively (see [21]). For first-order singular surfaces these restrictions are obtained as

$$[\![\boldsymbol{F}]\!] = \zeta\, \boldsymbol{m} \otimes \boldsymbol{N}, \qquad [\![\dot{\boldsymbol{x}}]\!] = -C\, \zeta\, \boldsymbol{m}, \tag{13}$$

where C denotes the velocity of propagation of $\partial_s\Omega$. Conditions (13) are associated with the development of shock waves. For the analysis of weak discontinuities, the compatibility conditions of second-order singular surfaces are required. From Eq. (13) they result in

$$[\![\mathrm{GRAD}\boldsymbol{F}]\!] = \zeta\, \boldsymbol{m} \otimes \boldsymbol{N} \otimes \boldsymbol{N}, \quad [\![\dot{\boldsymbol{F}}]\!] = -C\, \zeta\, \boldsymbol{m} \otimes \boldsymbol{N} \tag{14}$$

and

$$[\![\ddot{\boldsymbol{x}}]\!] = C^2\, \zeta\, \boldsymbol{m}. \tag{15}$$

Using Eq. $(14)_2$ together with $[\![\boldsymbol{F}]\!] = \boldsymbol{0}$ (second-order singular surface), the discontinuity of the spatial velocity gradient $\boldsymbol{l} := \dot{\boldsymbol{F}} \cdot \boldsymbol{F}^{-1}$ is computed as

$$[\![\boldsymbol{l}]\!] = [\![\dot{\boldsymbol{F}} \cdot \boldsymbol{F}^{-1}]\!] = [\![\dot{\boldsymbol{F}}]\!] \cdot \boldsymbol{F}^{-1} = -C\, \zeta\, \boldsymbol{m} \otimes \boldsymbol{N} \cdot \boldsymbol{F}^{-1} = \gamma\, \boldsymbol{m} \otimes \boldsymbol{n}, \tag{16}$$

with $\gamma := -C\, \zeta$. Eq. (16) represents the spatial counterpart of Eq. $(14)_2$.

3 WEAK DISCONTINUITIES

This section is concerned with a short summary of the localization condition associated with the development of weak discontinuities [3–5]. Consequently, the transition from $\boldsymbol{\varphi} \in C^\infty$ to $\boldsymbol{\varphi} \in C^0$ and $[\![\boldsymbol{F}]\!] \neq \boldsymbol{0}$ will be analyzed. Hence, the compatibility conditions (14), (15) and (16) have to be considered.

Starting with the continuity of the traction vector $\boldsymbol{T} := \boldsymbol{P} \cdot \boldsymbol{N}$ in the reference configuration in terms of the first PIOLA-KIRCHHOFF tensor $\boldsymbol{P}$ and assuming continuity of the tangent operator $\mathbb{C}^{\mathrm{ep}}$ ($\dot{\boldsymbol{P}} = \mathbb{C}^{\mathrm{ep}} : \dot{\boldsymbol{F}}$), the traction equilibrium reads

$$[\![\dot{\boldsymbol{T}}]\!] = \left[\dot{\boldsymbol{T}}^{+} - \dot{\boldsymbol{T}}^{-}\right] = \left(\mathbb{C}^{\mathrm{ep}} : [\![\dot{\boldsymbol{F}}]\!]\right) \cdot \boldsymbol{N} = -C\, \zeta\, \underbrace{(\boldsymbol{N} \cdot \mathbb{C}^{\mathrm{ep}} \cdot \boldsymbol{N})}_{\boldsymbol{Q}} \cdot \boldsymbol{m} = \boldsymbol{0}, \tag{17}$$

with

$$Q_{ik} = N_j\, \mathbb{C}_{ijkl}\, N_l. \tag{18}$$

Consequently, the non-trivial solution ($C\, \zeta\, \boldsymbol{m} \neq 0$) implies

$$\boxed{\det \boldsymbol{Q} = 0}\,. \tag{19}$$

Eq. (19) represents the localization condition of weak discontinuities formulated in the reference configuration.

From the identity of the forces described in the reference and in the current configuration

$$\overset{\circ}{\boldsymbol{\sigma}} \cdot \boldsymbol{n}\, \mathrm{d}a = \dot{\boldsymbol{P}} \cdot \boldsymbol{N}\, \mathrm{d}A, \tag{20}$$

the spatial counterpart of Eq. (19) reads

$$[\![\overset{\circ}{\boldsymbol{\sigma}}]\!] \cdot \boldsymbol{n} = \boldsymbol{0}. \tag{21}$$

In Eqs. (20) and (21), $\overset{\circ}{\boldsymbol{\sigma}}$ denotes the nonsymmetric nominal stress tensor. Inserting the rate form of the constitutive law

$$\overset{\circ}{\boldsymbol{\sigma}} = \overset{\circ}{\boldsymbol{c}}^{\mathrm{ep}} : \boldsymbol{l} \tag{22}$$

in terms of the fourth-order EULER tangent operator $\overset{\circ}{\boldsymbol{c}}^{\mathrm{ep}}$ together with the compatibility condition (16) into Eq. (22), yields

$$[\![\overset{\circ}{\boldsymbol{t}}]\!] = [\![\overset{\circ}{\boldsymbol{\sigma}}]\!] \cdot \boldsymbol{n} = \underbrace{\left(\boldsymbol{n} \cdot \overset{\circ}{\boldsymbol{c}}^{\mathrm{ep}} \cdot \boldsymbol{n}\right)}_{\boldsymbol{q}} \cdot \boldsymbol{m}\, \gamma = \boldsymbol{0} \tag{23}$$

with

$$q_{ik} = n_j \ \overset{\circ}{c}{}^{\mathrm{ep}}_{ijkl} \ n_l. \tag{24}$$

Eq. (23) represents the spatial counterpart of Eq. (19).

4 STRONG DISCONTINUITIES

After the classical localization condition associated with the formation of weak discontinuities has been summarized in Section 3, attention is focused on the development of strong discontinuities [9, 10]. More precisely, the transition from $\boldsymbol{\varphi} \in C^\infty$ to $\boldsymbol{\varphi} \in S$ and $\boldsymbol{\varphi} \notin C$ will be considered.

4.1 Kinematics at the onset of bifurcation

According to Section 2, the displacement field $\boldsymbol{u}$ at the onset of bifurcation is characterized by

$$\begin{array}{rcl} \boldsymbol{u} & = & \bar{\boldsymbol{u}} \\ \dot{\boldsymbol{u}} & = & \dot{\bar{\boldsymbol{u}}} + H_{\mathrm{s}}\, [\![\dot{\boldsymbol{u}}]\!] \end{array}, \quad \text{with} \quad \bar{\boldsymbol{u}} \in C^\infty(\Omega, \mathbb{R}^3), \quad [\![\dot{\boldsymbol{u}}]\!] \in C^\infty(\partial_{\mathrm{s}}\Omega, \mathbb{R}^3) \tag{25}$$

and

$$\begin{array}{rccl} H_{\mathrm{s}}: & \Omega & \rightarrow & \{0,1\} \\ & \boldsymbol{X} & \mapsto & \left\{ \begin{array}{ll} 1 & \forall \boldsymbol{X} \in \Omega^+ \\ 0 & \forall \boldsymbol{X} \in \Omega^- \cup \partial_{\mathrm{s}}\Omega. \end{array} \right. \end{array} \tag{26}$$

Assuming a spatially constant jump ($\mathrm{GRAD}[\![\dot{\boldsymbol{u}}]\!] = \boldsymbol{0}$), the rate of the deformation gradient is obtained as

$$\dot{\boldsymbol{F}} = \frac{\partial \dot{\boldsymbol{u}}}{\partial \boldsymbol{X}} = \underbrace{\frac{\partial \dot{\bar{\boldsymbol{u}}}}{\partial \boldsymbol{X}}}_{=:\, \dot{\bar{\boldsymbol{F}}}} + [\![\dot{\boldsymbol{u}}]\!] \otimes \boldsymbol{N}\, \delta_{\mathrm{s}}, \tag{27}$$

with the definition of the DIRAC-delta distribution δ_{s}

$$\delta_{\mathrm{s}}\, \boldsymbol{N} := \mathrm{GRAD} H_{\mathrm{s}}. \tag{28}$$

In Eq. (28), $\mathrm{GRAD} H_{\mathrm{s}}$ represents the generalized derivative of the HEAVISIDE function [22–24]. From Eq. (27), the spatial velocity gradient $\boldsymbol{l}$ is computed as

$$\boldsymbol{l} = \dot{\boldsymbol{F}} \cdot \boldsymbol{F}^{-1} = \dot{\boldsymbol{F}} \cdot \bar{\boldsymbol{F}}^{-1} = \underbrace{\dot{\bar{\boldsymbol{F}}} \cdot \bar{\boldsymbol{F}}^{-1}}_{=:\, \bar{\boldsymbol{l}}} + \underbrace{[\![\dot{\boldsymbol{u}}]\!] \otimes \boldsymbol{n}\, \delta_{\mathrm{s}}}_{=:\, \tilde{\boldsymbol{l}}}, \tag{29}$$

with

$$\boldsymbol{n} = \boldsymbol{N} \cdot \boldsymbol{F}^{-1} = \boldsymbol{N} \cdot \bar{\boldsymbol{F}}^{-1}. \tag{30}$$

Remark 1: *The additive decomposition (29) implies the introduction of an intermediate configuration. In contrast to computational finite strain plasticity, see e.g. [25, 26], the induced*

intermediate configuration is unique. To prove this, we start with a multiplicative split of the deformation gradient associated with a discontinuous displacement field ($\boldsymbol{\varphi} \notin C(\Omega, \mathbb{R}^3)$) according to [10, 27]

$$\boldsymbol{F} = \boldsymbol{1} + \frac{\partial \bar{\boldsymbol{u}}}{\partial \boldsymbol{X}} + [\![\boldsymbol{u}]\!] \otimes \boldsymbol{N}\, \delta_{\mathrm{s}} =: \bar{\boldsymbol{F}} \cdot \tilde{\boldsymbol{F}} \tag{31}$$

with

$$\begin{aligned} \bar{\boldsymbol{F}} &:= \boldsymbol{1} + \frac{\partial \bar{\boldsymbol{u}}}{\partial \boldsymbol{X}} \\ \tilde{\boldsymbol{F}} &:= \boldsymbol{1} + \underbrace{\bar{\boldsymbol{F}}^{-1} \cdot [\![\boldsymbol{u}]\!]}_{=:\,\boldsymbol{J}} \otimes \boldsymbol{N}\, \delta_{\mathrm{s}}. \end{aligned} \tag{32}$$

The gradient $\tilde{\boldsymbol{F}}$ represents the first-order approximation of the deformation from the reference to the intermediate configuration and the gradient $\bar{\boldsymbol{F}}$ from the intermediate to the current configuration, respectively. Since the initial conditions at the onset of bifurcation are given as

$$\begin{array}{l} [\![\boldsymbol{u}]\!] = \boldsymbol{0} \\ [\![\dot{\boldsymbol{u}}]\!] \neq \boldsymbol{0} \end{array} \quad \Rightarrow \quad \begin{aligned} \tilde{\boldsymbol{F}} &= \boldsymbol{1} \\ \dot{\tilde{\boldsymbol{F}}} &= \bar{\boldsymbol{F}}^{-1} \cdot [\![\dot{\boldsymbol{u}}]\!] \otimes \boldsymbol{N}\, \delta_{\mathrm{s}}, \end{aligned} \tag{33}$$

the rate of the deformation gradient results in

$$\dot{\boldsymbol{F}} = \dot{\bar{\boldsymbol{F}}} \cdot \tilde{\boldsymbol{F}} + \bar{\boldsymbol{F}} \cdot \dot{\tilde{\boldsymbol{F}}} = \dot{\bar{\boldsymbol{F}}} + [\![\dot{\boldsymbol{u}}]\!] \otimes \boldsymbol{N}\, \delta_{\mathrm{s}}. \tag{34}$$

Eq. (34) is equivalent to Eq. (27).

In summary, the kinematics at the onset of bifurcation are characterized by

$$\boldsymbol{F} = \bar{\boldsymbol{F}} \cdot \tilde{\boldsymbol{F}} \qquad \begin{array}{lcl} \bar{\boldsymbol{F}} = \dfrac{\partial \bar{\boldsymbol{u}}}{\partial \boldsymbol{X}} & \wedge & \dot{\bar{\boldsymbol{F}}} = \dfrac{\partial \dot{\bar{\boldsymbol{u}}}}{\partial \boldsymbol{X}} \\ \tilde{\boldsymbol{F}} = \boldsymbol{1} & \wedge & \dot{\tilde{\boldsymbol{F}}} = \boldsymbol{1} + \dot{\boldsymbol{J}} \otimes \boldsymbol{N}\, \delta_{\mathrm{s}}. \end{array} \tag{35}$$

For further derivations, it is convenient to decompose the LIE derivative of the displacement discontinuity

$$\mathcal{L}_{\boldsymbol{v}} [\![\boldsymbol{u}]\!] := [\![\dot{\boldsymbol{u}}]\!] - \bar{\boldsymbol{l}} \cdot [\![\boldsymbol{u}]\!] \tag{36}$$

relative to the intermediate configuration into a direction vector $\boldsymbol{m}$ and an amplitude ζ resulting in [10, 27, 28]

$$\mathcal{L}_{\boldsymbol{v}} [\![\boldsymbol{u}]\!] =: \dot{\zeta}\, \boldsymbol{m}, \quad ||\boldsymbol{m}||_2 = 1, \quad \dot{\zeta} := ||\mathcal{L}_{\boldsymbol{v}} [\![\boldsymbol{u}]\!]||_2. \tag{37}$$

Since the displacement discontinuity at the onset of bifurcation (see Eq. (25) and (35)) is zero, the intermediate configuration is identical to the reference configuration ($\tilde{\boldsymbol{F}} = \boldsymbol{1}$) and the identity

$$\mathcal{L}_{\boldsymbol{v}} [\![\boldsymbol{u}]\!] = [\![\dot{\boldsymbol{u}}]\!] = \dot{\zeta}\, \boldsymbol{m} \tag{38}$$

holds (see [17]).

Remark 2:*The assumption GRAD$[\![\dot{\boldsymbol{u}}]\!] = \boldsymbol{0}$ (see Eq. (27)) is motivated by the numerical implementation. In each integration point (or element) the displacement jump is assumed as constant [9, 10, 18, 19, 29, 30].*

4.2 Localization condition

In this subsection, the localization condition associated with the formation of strong discontinuities is derived in a general format without restricting to a special constitutive law. For that purpose, we start with a useful mathematical definition.

Let $\boldsymbol{Y}^{\boldsymbol{X}}$ be the set containing all mappings from $\boldsymbol{X}$ to $\boldsymbol{Y}$ and $\mathcal{DIR}(\boldsymbol{X},\boldsymbol{Y}) \subset \boldsymbol{Y}^{\boldsymbol{X}}$ the set of all singular distributions from $\boldsymbol{X}$ to $\boldsymbol{Y}$, then the mapping dirac : $\boldsymbol{Y}^{\boldsymbol{X}} \rightarrow \boldsymbol{Y}^{\boldsymbol{X}}$ is introduced according to

$$\text{dirac}: \begin{array}{lcl} \boldsymbol{Y}^{\boldsymbol{X}} & \rightarrow & \boldsymbol{Y}^{\boldsymbol{X}} \\ \boldsymbol{f} & \mapsto & \chi_{\mathcal{DIR}}\, \boldsymbol{f}. \end{array} \tag{39}$$

Following standard notations, $\chi_{\mathcal{Z}}$ represents the characteristic mapping corresponding to the set $\mathcal{Z} \subset \boldsymbol{Y}^{\boldsymbol{X}}$ defined by

$$\chi_{\mathcal{Z}}: \begin{array}{lcl} \boldsymbol{Y}^{\boldsymbol{X}} & \rightarrow & \{0,1\} \\ \mathcal{F} & \mapsto & \left\{ \begin{array}{ll} 1 & \forall \mathcal{F} \in \mathcal{Z} \\ 0 & \forall \mathcal{F} \notin \mathcal{Z} \end{array} \right. . \end{array} \tag{40}$$

Consequently, the mapping dirac : $\boldsymbol{Y}^{\boldsymbol{X}} \rightarrow \boldsymbol{Y}^{\boldsymbol{X}}$ represents the identity on $\mathcal{DIR}$ and vanishes for all regularly distributed mappings. For a better understanding of the introduced notation, the dirac mapping is applied to the spatial velocity gradient $\boldsymbol{l}$ resulting in

$$\text{dirac}(\boldsymbol{l}) = \text{dirac}(\bar{\boldsymbol{l}} + \tilde{\boldsymbol{l}}) = \text{dirac}(\tilde{\boldsymbol{l}}) = \tilde{\boldsymbol{l}}. \tag{41}$$

The bifurcation conditions (19) and (23) are based on the traction equilibrium at the singular surface $\partial_{\text{s}}\Omega$. However, starting with a discontinuous displacement field, which results in singularly distributed strains, the boundedness of the stress field at the localization surface has to be fulfilled [9]. Since the singular strains are restricted to the material surface $\partial_{\text{s}}\Omega$, the stresses in $\Omega^{\pm}$ follow from regularly distributed strains and consequently, they are regularly distributed, too. Therefore the localization condition corresponding to the formation of strong discontinuities reads

$$\text{dirac}\left[\dot{\boldsymbol{T}}|_{\partial_{\text{s}}\Omega}\right] = 0. \tag{42}$$

Using the regular distribution of the tractions in $\Omega^{\pm}$, Eq. (42) can be rewritten as

$$\boxed{\text{dirac}\left[\dot{\boldsymbol{T}}^{+} - \dot{\boldsymbol{T}}|_{\partial_{\text{s}}\Omega}\right] = 0}\,. \tag{43}$$

Localization condition (43) is formally identical to Eq. (17). Applying the CAUCHY lemma, Eq. (42) results in

$$\text{dirac}\left[\dot{\boldsymbol{P}}|_{\partial_{\text{s}}\Omega}\right] \cdot \boldsymbol{N} = 0. \tag{44}$$

In Eq. (44), the material character of the singular surface $\dot{\boldsymbol{N}} = \boldsymbol{0}$ has been used. However, for a computational framework, Eq. (44) is not suitable. With the transformation relation between the second PIOLA-KIRCHHOFF stress tensor $\boldsymbol{S}$ and the first PIOLA-KIRCHHOFF stress tensor $\boldsymbol{P} = \boldsymbol{F} \cdot \boldsymbol{S}$, the localization condition is obtained as

$$\text{dirac}\left[\dot{\boldsymbol{P}}|_{\partial_{\text{s}}\Omega}\right] \cdot \boldsymbol{N} = \boxed{\left[\bar{\boldsymbol{F}} \cdot \dot{\tilde{\boldsymbol{F}}} \cdot \boldsymbol{S} + \bar{\boldsymbol{F}} \cdot \text{dirac}\left[\dot{\boldsymbol{S}}\right]\right]\Big|_{\partial_{\text{s}}\Omega} \cdot \boldsymbol{N} = 0}\,. \tag{45}$$

Alternatively, the localization condition (45) can be rewritten into its EULERian counterpart. Applying the transformation $\boldsymbol{n} = \boldsymbol{N} \cdot \bar{\boldsymbol{F}}^{-1}$ together with the LIE derivative of the KIRCHHOFF stresses $\mathcal{L}_{\boldsymbol{v}}\boldsymbol{\tau} := \bar{\boldsymbol{F}} \cdot \dot{\boldsymbol{S}} \cdot \bar{\boldsymbol{F}}^{T}$, the localization condition in the deformed configuration reads

$$\boxed{\left[\tilde{\boldsymbol{l}} \cdot \boldsymbol{\tau} + \text{dirac}\left[\mathcal{L}_{\boldsymbol{v}}\boldsymbol{\tau}\right]\right]\Big|_{\partial_{\text{s}}\Omega} \cdot \boldsymbol{n} = 0}\,. \tag{46}$$

In Eq. (46), the identity $\tilde{\boldsymbol{l}} = \bar{\boldsymbol{F}} \cdot \dot{\tilde{\boldsymbol{F}}} \cdot \bar{\boldsymbol{F}}^{-1}$, which follows directly from Eq. (29), (30), (31) and (31) has been used.

4.3 Anisotropic elastoplasticity

So far, our derivations hold without loss of generality. However, the rates of the stress tensors $\boldsymbol{S}$ (see Eq. (45)) and $\boldsymbol{\tau}$ (see Eq. (46)), respectively, depend on the mechanical behavior of the considered material. Consequently, in this subsection Eq. (46) is specified for a particular material model.

The condition corresponding to the formation of strong discontinuities has been derived in the case of a geometrically linear theory for isotropic and anisotropic damage models as well as for non-associated plasticity theory (see e.g. [9, 18, 31, 32]). The counterparts for plasticity models at finite strains were proposed in [10, 33]. Using an approximation of the DIRAC-delta distribution $\delta_{\mathrm{s}} \approx 1/k$ by means of a constant coefficient k (regularized strong discontinuity), an alternative condition was suggested in [34]. However, this regularized version will not be considered throughout the rest of this paper. The derivations presented in [10, 33] are based on the multiplicative split of the deformation gradient $\boldsymbol{F} = \boldsymbol{F}^{\mathrm{e}} \cdot \boldsymbol{F}^{\mathrm{p}}$ into an elastic and a plastic part and a yield criterion formulated in terms of KIRCHHOFF stresses. Since in this references softening evolution has been assumed to be isotropic and furthermore, no structural tensors have been considered, only isotropic yield functions are admissible.

In this subsection, we re-formulate the bifurcation condition for anisotropic materials using unregularized strong discontinuities. For that purpose, we use a recently suggested framework for finite strain plasticity. This approach falls into the range of the rate-independent plasticity theory of GREEN & NAGHDI [35] and has been proposed by [15, 16] and further elaborated by [36, 37]. Clearly, other frameworks such as the multiplicative decomposition of the deformation gradient, cf. [38], or the additive decomposition of the spatial rate of deformation tensor, see [39], are suitable as well.

The key assumption of the plasticity model considered is the additive split of the strains into elastic and plastic parts, analogously to the geometrically linear theory. This additive decomposition approximates the multiplicative split of the deformation gradient best, if logarithmic strains

$$\boldsymbol{E} = \frac{1}{2} \ln \boldsymbol{C}, \quad \text{with} \quad \boldsymbol{C} = \boldsymbol{F}^T \cdot \boldsymbol{F} \tag{47}$$

are used. The resulting constitutive model is summarized in Table 1. According to Table 1, initial anisotropy is governed by structural tensors ${}^{i}\boldsymbol{M}$. Following [16, 36, 37], the consistency condition reads

$$\dot{\phi} = \partial_{\hat{\boldsymbol{S}}} \phi : \hat{\dot{\boldsymbol{S}}} + \partial_{\boldsymbol{B}} \phi : \dot{\boldsymbol{B}} + \partial_{q} \phi \, \dot{q} = 0. \tag{48}$$

If we require the stress fields to be in $\mathcal{B}(\mathbb{R}^3, \mathbb{R}^6)$ (bounded mapping from $\boldsymbol{X}$ to $\mathbb{R}^6$) the stress-like internal variables $\boldsymbol{B}$ and q have to be bounded as well. Consequently,

$$\mathrm{dirac}\,[\boldsymbol{B}] = \boldsymbol{0} \quad \text{and} \quad \mathrm{dirac}\,[q] = 0. \tag{49}$$

For further details we refer to [9, 10, 18]. Inserting Eqs. (49) into the consistency condition (48) and applying the dirac-mapping as introduced in Def. (39), results in

$$\mathrm{dirac}\left[\dot{\phi}\right] = \mathrm{dirac}\left[\partial_{\hat{\boldsymbol{S}}} \phi : \hat{\dot{\boldsymbol{S}}}\right] = \partial_{\hat{\boldsymbol{S}}} \phi : \mathrm{dirac}\left[\hat{\dot{\boldsymbol{S}}}\right] = 0. \tag{50}$$

From Eq. (50), together with the stress rates (see Table 1),

$$\hat{\dot{\boldsymbol{S}}} = \partial_{\boldsymbol{E}^{\mathrm{e}} \otimes \boldsymbol{E}^{\mathrm{e}}} \psi : \left(\dot{\boldsymbol{E}} - \dot{\boldsymbol{E}}^{\mathrm{p}} \right), \tag{51}$$

the plastic multiplier is computed as

$$\mathrm{dirac}\,[\lambda] = \frac{\partial_{\hat{\boldsymbol{S}}} \phi : \partial_{\boldsymbol{E}^{\mathrm{e}} \otimes \boldsymbol{E}^{\mathrm{e}}} \psi : \mathrm{dirac}\left[\dot{\boldsymbol{E}}\right]}{\partial_{\hat{\boldsymbol{S}}} \phi : \partial_{\boldsymbol{E}^{\mathrm{e}} \otimes \boldsymbol{E}^{\mathrm{e}}} \psi : \partial_{\hat{\boldsymbol{S}}} g}. \tag{52}$$

Strain tensor	$\boldsymbol{E} = \frac{1}{2}\,\ln \boldsymbol{C}, \quad \boldsymbol{C} = \boldsymbol{F}^T \cdot \boldsymbol{F}$
Additive split	$\boldsymbol{E} = \boldsymbol{E}^{\mathrm{e}} + \boldsymbol{E}^{\mathrm{p}}$
Internal variables	$\mathcal{I} := \{\boldsymbol{E}^{\mathrm{p}}, \boldsymbol{A}, \alpha\}$
Structural tensors	${}^i\boldsymbol{M} =^i \boldsymbol{a} \otimes^i \boldsymbol{a}$
Free energy	$\psi = \psi(\boldsymbol{E}^{\mathrm{e}}, \boldsymbol{A}, \alpha, {}^i\boldsymbol{M})$
Stress tensor	$\hat{\boldsymbol{S}} = \partial_{\boldsymbol{E}^{\mathrm{e}}}\psi$
Back stress	$\boldsymbol{B} = \partial_{\boldsymbol{A}}\psi$
Isotropic hardening	$q = \partial_\alpha \psi$
Relative stresses	$\boldsymbol{\Sigma} = \hat{\boldsymbol{S}} - \boldsymbol{B}$
Yield function	$\phi(\boldsymbol{\Sigma}, {}^i\boldsymbol{M}, q)$
Flow rule	$\dot{\boldsymbol{E}}^{\mathrm{p}} = \lambda\, \partial_{\hat{\boldsymbol{S}}} g(\boldsymbol{\Sigma}, {}^i\boldsymbol{M}, q)$
Evolution of $\boldsymbol{A}$	$\dot{\boldsymbol{A}} = -\lambda\, \partial_{\hat{\boldsymbol{S}}} h(\boldsymbol{\Sigma}, {}^i\boldsymbol{M}, q)$
Evolution of α	$\dot{\alpha} = \lambda\, \partial_q h(\boldsymbol{\Sigma}, {}^i\boldsymbol{M}, q)$

Table 1: Anisotropic plasticity model (see [16, 36, 37]))

As a consequence, the plastic multiplier represents a singular distribution (see [9]).

Remark 3:*Eq. (52) holds independently on the loading conditions in* $\Omega^{\pm}$. *Only the boundedness of the stresses is required. Note, that Eq. (52) does not imply* $\lambda = \lambda_\delta\ \delta_{\mathrm{s}}$. *The more general case* $\lambda = \bar{\lambda} + \lambda_\delta\ \delta_{\mathrm{s}}$, *with* $\bar{\lambda} \neq 0$ *and dirac*$[\bar{\lambda}] = 0$ *also results in Eq. (52).*

Inserting the singularly distributed part of the plastic multiplier together with the evolution of the plastic strains (see Table 1) into Eq. (51), the singularly distributed part of the stresses is obtained as

$$\text{dirac}\left[\dot{\hat{\boldsymbol{S}}}\right] = \hat{\mathbb{C}}^{\text{perf}} : \text{dirac}\left[\dot{\boldsymbol{E}}\right]. \tag{53}$$

with the fourth-order constitutive tensor defined as

$$\hat{\mathbb{C}}^{\text{perf}} = \partial_{\boldsymbol{E}^{\mathrm{e}} \otimes \boldsymbol{E}^{\mathrm{e}}}\psi - \frac{\partial_{\boldsymbol{E}^{\mathrm{e}} \otimes \boldsymbol{E}^{\mathrm{e}}}\psi : \partial_{\hat{\boldsymbol{S}}} g \otimes \partial_{\hat{\boldsymbol{S}}}\phi : \partial_{\boldsymbol{E}^{\mathrm{e}} \otimes \boldsymbol{E}^{\mathrm{e}}}\psi}{\partial_{\hat{\boldsymbol{S}}}\phi : \partial_{\boldsymbol{E}^{\mathrm{e}} \otimes \boldsymbol{E}^{\mathrm{e}}}\psi : \partial_{\hat{\boldsymbol{S}}} g}. \tag{54}$$

$\hat{\mathbb{C}}^{\text{perf}}$ represents the perfect plastic tangent operator.

So far our derivations are based on logarithmic strains $\boldsymbol{E}$ and the conjugate stresses $\hat{\boldsymbol{S}}$. However, the conditions (45) and (46) are formulated in terms of $\boldsymbol{S}$ and $\boldsymbol{\tau}$, respectively. Consequently, Eq. (53) has to be transformed. For that purpose, the projections defined in Table 2 are applied. Explicit formulas for $\mathbb{P}$ and $\mathbb{L}$ can be found in [36, 37]. According to Table 2, at first the second PIOLA-KIRCHHOFF stresses $\boldsymbol{S}$ are computed in terms of $\hat{\boldsymbol{S}}$. Note, that both stresses are defined with respect to the reference configuration. In a second step, a full push forward is applied. By this, the singular part of the LIE derivative of the KIRCHHOFF stresses results in

$$\text{dirac}\left[\mathcal{L}_{\boldsymbol{v}}\boldsymbol{\tau}\right] = \mathbb{C}^{\text{perf}}_{\mathrm{E}} : \text{dirac}\left[\boldsymbol{d}\right], \quad \text{with} \quad \boldsymbol{d} = \text{sym}\left[\boldsymbol{l}\right]. \tag{55}$$

Using Eq. (29), which results in the identity

$$\text{dirac}\left[\boldsymbol{d}\right] = \text{sym}\left[\tilde{\boldsymbol{l}}\right], \tag{56}$$

the localization condition (46) is rewritten as

$$\underbrace{\left[\boldsymbol{n} \cdot \mathbb{C}^{\text{perf}}_{\mathrm{E}} \cdot \boldsymbol{n} + \boldsymbol{n} \cdot \boldsymbol{\tau} \cdot \boldsymbol{n}\, \boldsymbol{1}\right]}_{\boldsymbol{q}^{\text{perf}}} \cdot [\![\dot{\boldsymbol{u}}]\!] = \boldsymbol{0}. \tag{57}$$

Tangent moduli	
with respect to the stresses $\hat{\boldsymbol{S}}$	$\dot{\hat{\boldsymbol{S}}} = \hat{\mathbb{C}}^{\text{ep}} : \dot{\boldsymbol{E}}$
with respect to 2nd PIOLA-KIRCHHOFF stresses	$\dot{\boldsymbol{S}} = \mathbb{C}_{\text{L}}^{\text{ep}} : \frac{1}{2}\dot{\boldsymbol{C}}$
	$\mathbb{C}_{\text{L}}^{\text{ep}} = \mathbb{P}_{\text{L}}^{T} : \hat{\mathbb{C}}^{\text{ep}} : \mathbb{P}_{\text{L}} + \hat{\boldsymbol{S}} : \mathbb{L}_{\text{L}}$
with respect to KIRCHHOFF stresses	$\mathcal{L}_{\boldsymbol{v}}\boldsymbol{\tau} = \mathbb{C}_{\text{E}}^{\text{ep}} : \boldsymbol{d}$
	$[\mathbb{C}_{\text{E}}^{\text{ep}}]_{abcd} = F_{aA}\, F_{bB}\, F_{cC}\, F_{dD}\, [\mathbb{C}_{\text{L}}^{\text{ep}}]_{ABCD}$
Projection tensors	
Projection tensor $\mathbb{P}_{\text{L}}$	$\mathbb{P}_{\text{L}} := 2\, \partial_{\boldsymbol{C}} \boldsymbol{E}$
Projection tensor $\mathbb{L}_{\text{L}}$	$\mathbb{L}_{\text{L}} := 4\, \partial_{\boldsymbol{C} \otimes \boldsymbol{C}} \boldsymbol{E}$

Table 2: Projection (see [36, 37]))

The non-trivial solution of Eq. (57) characterized by $[\![\dot{\boldsymbol{u}}]\!] \neq \boldsymbol{0}$ is given by

$$\boxed{\det \boldsymbol{q}^{\text{perf}} = 0}\,. \tag{58}$$

In contrast to Eq. (23) and (19), Eq. (58) is based on the perfect plastic acoustic tensor $\boldsymbol{q}^{\text{perf}}$ [9].

5 NUMERICAL BIFURCATION ANALYSES

This section is concerned with the development of an efficient algorithm for the computation of the localization mode of weak and strong discontinuities. Since the localization conditions (23) and (58) are formally identical, the suggested algorithmic formulation is suitable for both types of discontinuities.

To the best knowledge of the author, numerical bifurcation analyses have been proposed primarily in [13, 14]. Despite the efficiency of these numerical models, some modifications and extensions are necessary. The two-dimensional implementation as proposed in [13, 14] is based directly on Eq. (23). Due to finite load steps in computational analyses, it is possible, that bifurcation does not take place in a material point neither at time t_n ($\det \boldsymbol{q} > 0$) nor at time t_{n+1} ($\det \boldsymbol{q} < 0$). Consequently, the condition $\det \boldsymbol{q} = 0$ never occurs. In fact, it is more appropriate to consider the optimization problem

$$\boldsymbol{n} = \arg\left(\min_{\boldsymbol{n}} \ \det \boldsymbol{q}(\boldsymbol{n})\right) \tag{59}$$

under the constraints

$$\det \boldsymbol{q} \leq 0 \qquad \wedge \qquad ||\boldsymbol{n}||_2 = 1. \tag{60}$$

Again, Eqs. (59) and (60) have been primarily suggested in [13, 14]. However, the presented derivations in [13, 14] are based on a symmetric acoustic tensor. This implies an associative flow rule. Our proposed implementation does not require this restriction and differs completely from the one in [13, 14].

According to [13, 14], the minimum of $\det \boldsymbol{q}$ has to be determined in a first step. Afterwards it is checked, if $\det \boldsymbol{q} \leq 0$. For the computation of Eq. (59) under the constraint $(60)_2$, different concepts can be applied. Following standard optimization techniques (see e.g. [40, 41]), the constraint (60) can be taken into account by using a penalty formulation, LAGRANGE factors or by using spherical coordinates. In [13, 14] LAGRANGE's method has been applied. However, in

this case the nonlinear set of equations consists of 4 unknowns (three components of the vector $\boldsymbol{n}$ and a LAGRANGE multiplier). In contrast to [13, 14], we use spherical coordinates resulting in

$$\boldsymbol{n} = \begin{bmatrix} \sin\alpha\ \cos\theta \\ \sin\alpha\ \sin\theta \\ \cos\alpha \end{bmatrix} \Rightarrow \frac{\partial \boldsymbol{n}}{\partial \alpha} = \begin{bmatrix} \cos\alpha\ \cos\theta \\ \cos\alpha\ \sin\theta \\ -\sin\alpha \end{bmatrix}, \frac{\partial \boldsymbol{n}}{\partial \theta} = \begin{bmatrix} -\sin\alpha\ \sin\theta \\ \sin\alpha\ \cos\theta \\ 0 \end{bmatrix}, \tag{61}$$

with $(\alpha, \theta) \in [0, 2\,\pi] \times [0, \pi]$. Hence, the number of unknowns reduces to two. Using the chain rule, the necessary stationary condition corresponding to an extremum reads

$$\begin{aligned} \frac{\partial f}{\partial \alpha} &= \frac{\partial f}{\partial \boldsymbol{n}} \cdot \frac{\partial \boldsymbol{n}}{\partial \alpha} = 0 \\ \frac{\partial f}{\partial \theta} &= \frac{\partial f}{\partial \boldsymbol{n}} \cdot \frac{\partial \boldsymbol{n}}{\partial \theta} = 0, \end{aligned} \qquad \begin{aligned} \boldsymbol{q} &= \boldsymbol{n} \cdot \mathbb{C} \cdot \boldsymbol{n} \\ f &:= \det \boldsymbol{q}(\boldsymbol{n}(\alpha, \theta)). \end{aligned} \tag{62}$$

As a consequence and analogously to [13, 14], the derivative of f with respect to $\boldsymbol{n}$ has to be computed. Introducing the third-order tensor (see Remark **??**)

$$\mathcal{C}_{ijk} := \mathbb{C}_{kijl}\, n_l + n_l\, \mathbb{C}_{lijk}, \tag{63}$$

by means of its components, the derivative is obtained as

$$\frac{\partial f}{\partial \boldsymbol{n}} = f\ \boldsymbol{q}^{-T} : \mathcal{C}. \tag{64}$$

In contrast to [13, 14], the tangent operator $\mathbb{C}$ is not restricted by the condition of major symmetry. Only for associative evolution equations Eq. (64) is equivalent to its counterpart in [13, 14]. For the computation of the minimum of Eq. (59), we consider the nonlinear optimization problem

$$\boldsymbol{r} = \begin{bmatrix} \dfrac{\partial f}{\partial \alpha} \\ \dfrac{\partial f}{\partial \theta} \end{bmatrix} = \boldsymbol{0}. \tag{65}$$

The roots of Eq. (65) are computed using NEWTON's method based on the consistent linearization of Eq. (65). Hence, the iterative procedure

$$\boldsymbol{r}|_k + \underbrace{\left[\begin{array}{cc} \dfrac{\partial^2 f}{\partial \alpha^2} & \dfrac{\partial^2 f}{\partial \alpha \partial \theta} \\ \text{sym} & \dfrac{\partial^2 f}{\partial \theta^2} \end{array}\right]\Bigg|_k}_{\boldsymbol{R}|_k} \underbrace{\begin{bmatrix} \Delta\alpha \\ \Delta\theta \end{bmatrix}\Bigg|_{k+1}}_{\boldsymbol{\Delta}} = \boldsymbol{0} \tag{66}$$

is applied. In Eq. (66), the index k indicates the number of the iterative step. Since $\det \boldsymbol{q} \in C^\infty[[0, 2\pi] \times [0, \pi], \mathbb{R}]$, the second partial derivatives in Eq. (66) are well defined and the symmetry $(\partial^2 f)/(\partial\alpha\partial\theta) = (\partial^2 f)/(\partial\theta\partial\alpha)$ holds. Applying the chain rule, we obtain

$$\begin{aligned} \frac{\partial^2 f}{\partial \alpha^2} &= \frac{\partial^2 f}{\partial \boldsymbol{n} \otimes \partial \boldsymbol{n}} : \left(\frac{\partial \boldsymbol{n}}{\partial \alpha} \otimes \frac{\partial \boldsymbol{n}}{\partial \alpha}\right) + \frac{\partial f}{\partial \boldsymbol{n}} \cdot \frac{\partial^2 \boldsymbol{n}}{\partial \alpha^2} \\ \frac{\partial^2 f}{\partial \theta^2} &= \frac{\partial^2 f}{\partial \boldsymbol{n} \otimes \partial \boldsymbol{n}} : \left(\frac{\partial \boldsymbol{n}}{\partial \theta} \otimes \frac{\partial \boldsymbol{n}}{\partial \theta}\right) + \frac{\partial f}{\partial \boldsymbol{n}} \cdot \frac{\partial^2 \boldsymbol{n}}{\partial \theta^2} \\ \frac{\partial^2 f}{\partial \alpha \partial \theta} = \frac{\partial^2 f}{\partial \theta \partial \alpha} &= \frac{\partial^2 f}{\partial \boldsymbol{n} \otimes \partial \boldsymbol{n}} : \left(\frac{\partial \boldsymbol{n}}{\partial \alpha} \otimes \frac{\partial \boldsymbol{n}}{\partial \theta}\right) + \frac{\partial f}{\partial \boldsymbol{n}} \cdot \frac{\partial^2 \boldsymbol{n}}{\partial \alpha \partial \theta}, \end{aligned} \tag{67}$$

with

$$\frac{\partial^2 \boldsymbol{n}}{\partial \alpha^2} = \begin{bmatrix} -\sin\alpha\cos\theta \\ -\sin\alpha\sin\theta \\ -\cos\alpha \end{bmatrix}, \quad \frac{\partial^2 \boldsymbol{n}}{\partial \theta^2} = \begin{bmatrix} -\sin\alpha\cos\theta \\ -\sin\alpha\sin\theta \\ 0 \end{bmatrix}, \quad \frac{\partial^2 \boldsymbol{n}}{\partial \alpha \partial \theta} = \begin{bmatrix} -\cos\alpha\sin\theta \\ \cos\alpha\cos\theta \\ 0 \end{bmatrix}. \tag{68}$$

After some algebraic manipulations, the second derivatives of f with respect to $\boldsymbol{n}$ are decomposed additively according to

$$\boldsymbol{F} = \frac{\partial^2 f}{\partial \boldsymbol{n} \otimes \partial \boldsymbol{n}} = \boldsymbol{A} + \boldsymbol{B} + \boldsymbol{C} + \boldsymbol{C}^T = \boldsymbol{F}^T, \tag{69}$$

with the second-order tensors $\boldsymbol{A}$, $\boldsymbol{B}$ and $\boldsymbol{C}$ defined by

$$\boldsymbol{A} := \frac{\partial f}{\partial \boldsymbol{n}} \otimes \boldsymbol{q}^{-T} : \mathcal{C} = f\ \boldsymbol{q}^{-T} : \mathcal{C} \otimes \boldsymbol{q}^{-T} : \mathcal{C} = \boldsymbol{A}^T, \tag{70}$$

$$\boldsymbol{B} := f\ \left(\frac{\partial \boldsymbol{q}^{-T}}{\partial \boldsymbol{q}} : \mathcal{C} \right) : \mathcal{C} = \boldsymbol{B}^T, \quad \text{with} \quad \frac{\partial q_{ij}^{-T}}{\partial q_{kl}} = -q_{jk}^{-1}\ q_{li}^{-1} \tag{71}$$

and

$$\boldsymbol{C} := f\ \boldsymbol{q}^{-T} : \mathbb{C} \qquad C_{ij} = f\ q_{kl}^{-T} \mathbb{C}_{iklj}. \tag{72}$$

The initial value of the iterative NEWTON algorithm $\hat{\boldsymbol{n}}^*$ is computed by means of

$$\hat{\boldsymbol{n}}^* = \arg\left(\min_{\boldsymbol{n}(\alpha,\theta)} \det \boldsymbol{q}_{\mathrm{perf}}(\boldsymbol{n}) \right)\Big|_{(\alpha,\theta)\in\mathbb{A}}, \tag{73}$$

In Eq. (73), the definition

$$\mathbb{A} := \left\{ \frac{2\Pi\, i}{K} \;\middle|\; i \in \mathbb{N} \cup \{0\};\ i \leq K \right\}^2. \tag{74}$$

has been used. According to Eq. (74), the parameter K controls the number of discrete points.

Remark 4:*Note that the domain $\boldsymbol{A} := [0, 2\pi] \times [0, \pi]$ represents a compact set and $f = det\boldsymbol{q}(\alpha, \theta) \in C^\infty(\boldsymbol{A}, \mathbb{R})$. Hence, the minimum of f exists.*

Remark 5:For computational analyses, it is convenient to ,,normalize" the function f by means of the determinant of the elastic acoustic tensor. In the case of isotropic elasticity, the simplification $\det \boldsymbol{q}^{\mathrm{el}}(\boldsymbol{n}) = const\ \forall \boldsymbol{n} \in S^2$ holds ($\mathcal{S}^n$ represents the n-sphere). For the linearized theory

$$\det \boldsymbol{q}^{\mathrm{el}}(\boldsymbol{n}) = \det \boldsymbol{q}^{\mathrm{el}}((1,0,0)^T) = (2\mu + \Lambda)\ \mu^2 \tag{75}$$

follows. In Eq. (75), μ and Λ represent the LAME *constants.*

Remark 6:*According to Eq. (23), the simple contractions of the vector $\boldsymbol{n}$ with the constitutive tangent operator are applied with respect to the second and the fourth component. This differs from Eq. (62) and (63), respectively. However, introducing the fourth order tensor $\mathbb{C}$ via $\mathbb{C}_{ijkl} := \mathbb{C}^{\mathrm{ep}}_{jikl}$ this inconsistency is bypassed.*

NEWTON's method represents an efficient tool for the computation of roots of nonlinear equations due to its asymptotic quadratic convergence. However, if the initial value is far away from this root, numerical problems may arise [40–43]. An efficient strategy to enlarge the radius of convergence is represented by the line search algorithm. In contrast to the standard update

$$\begin{bmatrix} \alpha \\ \theta \end{bmatrix}\Big|_{k+1} = \begin{bmatrix} \alpha \\ \theta \end{bmatrix}\Big|_{k} + \beta\ \boldsymbol{\Delta}|_{k+1}, \quad \beta = 1 \tag{76}$$

of NEWTON's method, the damping coefficient β is determined according to

$$\beta = \arg\min_{\kappa}(\det \boldsymbol{q}(\boldsymbol{n}((\alpha,\theta)|_k + \kappa\ \boldsymbol{\Delta}|_{k+1}))). \tag{77}$$

In the presented implementation we have approximated the mapping $\det \boldsymbol{q}(\kappa) : \mathbb{R} \rightarrow \mathbb{R}$ using a quadratic function g characterized by $g(a_i) = \det \boldsymbol{q}(\kappa = a_i)$ with $a_i \in \mathbb{R}$ and $i \in \{1,2,3\}$. For the minimum of the quadratic function g a closed form solution is known. The resulting algorithm is summarized in Fig. 2.

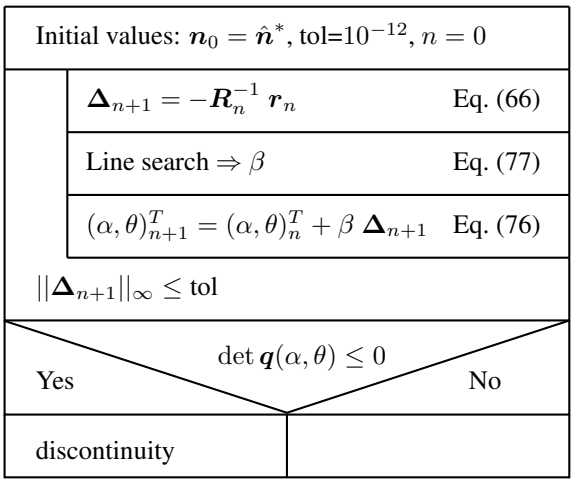

Figure 2: Numerical bifurcation analysis: Structure chart

6 NUMERICAL EXAMPLES

The applicability of the proposed implementation as well as its performance and numerical robustness is investigated by means of three-dimensional numerical bifurcation analyses. For a comparison of the numerically computed results with closed form solutions reported in [44], a geometrically linearized DRUCKER-PRAGER type plasticity model described in Table 3 is considered. Since the proposed implementation is identical for geometrically linear theories and finite deformations, the presented numerical analyses are meaningful.

The material model is summarized in Table 3. In Table 3, E denotes the YOUNG's modulus, ν the POISSON's ration, $\sigma_{\text{eq}}^{\text{ini}}$ an equivalent initial strength, and α_1 and α_2 two variables effecting the hydrostatic stress part of the yield function and the plastic potential, respectively. According to [44], α_1 and $\sigma_{\text{eq}}^{\text{ini}}$ are related to the uniaxial compression strength f_{c} and the uniaxial tensile strength f_{tu}

$$\alpha_1 = \frac{f_{\text{c}} - f_{\text{tu}}}{\sqrt{3}\ (f_{\text{c}} + f_{\text{tu}})} \quad \text{and} \quad \sigma_{\text{eq}}^{\text{ini}} = \frac{2\ f_{\text{c}}\ f_{\text{tu}}}{\sqrt{3}\ (f_{\text{c}} + f_{\text{tu}})}. \tag{78}$$

Following [44], α_2 is set to zero. Consequently, the plastic potential is of VON MISES type.

The applicability of the proposed implementation as well as its performance is investigated by the analyses of two different load cases. At first, we apply the stress state

$$\boldsymbol{\sigma} = \sigma\ \boldsymbol{e}_3 \otimes \boldsymbol{e}_3, \quad \text{with} \quad \sigma < 0. \tag{79}$$

In Eq. (79), $\boldsymbol{e}_i$ denote the Cartesian bases. The shape of the yield function and the plastic potential, respectively, are specified by setting $f_{\text{c}} = 2.0$ and $f_{\text{tu}} = 1.0$. The ratio between the

Total strains	$\boldsymbol{\varepsilon} = \text{sym}[\text{GRAD}\boldsymbol{u}]$
Elastic strains	$\boldsymbol{\varepsilon}^{\text{e}} = \boldsymbol{\varepsilon} - \boldsymbol{\varepsilon}^{\text{p}}$
Free energy	$\psi(\boldsymbol{\varepsilon}^{\text{e}}, \alpha) = \frac{1}{2}\,\frac{E}{1+\nu}\,\boldsymbol{\varepsilon}^{\text{e}} : \boldsymbol{\varepsilon}^{\text{e}} + \frac{1}{2}\,\frac{E\,\nu}{(1+\nu)(1-2\,\nu)}(\boldsymbol{\varepsilon}^{\text{e}} : \mathbf{1})^2 + \psi_{\text{in}}(\alpha)$
Stress tensor	$\boldsymbol{\sigma} = \partial_{\boldsymbol{\varepsilon}^{\text{e}}}\psi = \partial_{\boldsymbol{\varepsilon}^{\text{e}}\otimes\boldsymbol{\varepsilon}^{\text{e}}}\psi : \boldsymbol{\varepsilon}^{\text{e}}$
Isotropic hardening	$q = \partial_\alpha \psi$
Yield function	$\phi(\boldsymbol{\sigma}, q) = \sqrt{J_2} + \alpha_1\,\boldsymbol{\sigma} : \mathbf{1} - \sigma_{\text{eq}}^{\text{ini}} + q(\alpha), \quad J_2 := \text{dev}[\boldsymbol{\sigma}] : \text{dev}[\boldsymbol{\sigma}]$
Plastic potential	$g(\boldsymbol{\sigma}, q) = \sqrt{J_2} + \alpha_2\,\boldsymbol{\sigma} : \mathbf{1} - \sigma_{\text{eq}}^{\text{ini}} + q(\alpha)$
Flow rule	$\dot{\boldsymbol{\varepsilon}}^{\text{p}} = \lambda\,\partial_{\boldsymbol{\sigma}} g$
Evolution of α	$\dot{\alpha} = \lambda\,\partial_q g$

Table 3: DRUCKER-PRAGER type non-associative plasticity model (geometrically linear).

YOUNG's modulus E and the softening modulus $H := -\partial q/\partial\alpha$ is assumed as $H/E = 0.125$. The chosen parameters are identical to those reported in [44]. An illustration of the computed determinant of the acoustic tensor is given in Fig. 3. Fig. 3b contains a Cartesian illustration of

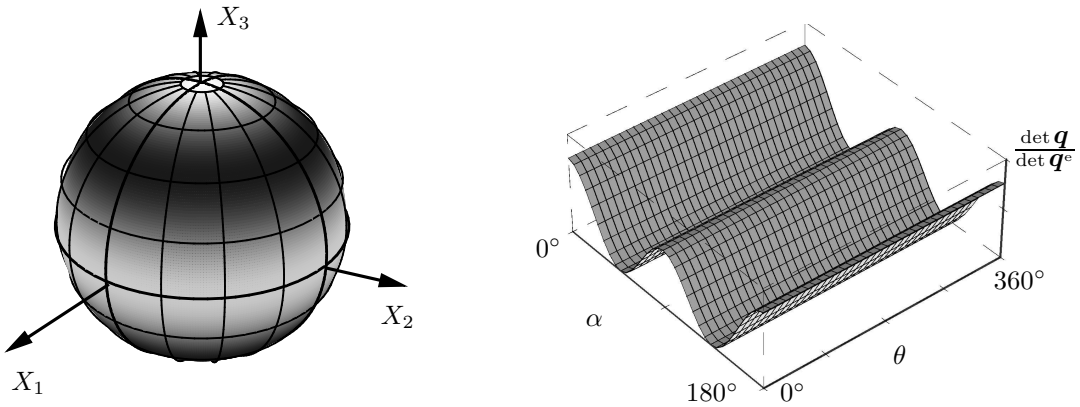

a) b)

Figure 3: Numerical bifurcation analysis: Determinant of the acoustic tensor (normalized): DRUCKER-PRAGER type plasticity model (see Table 3); uniaxial compression $\boldsymbol{\sigma} = \sigma\,\boldsymbol{e}_3 \otimes \boldsymbol{e}_3$; $\nu = 0.2$: a) Spherical illustration (white $:\Leftrightarrow \det \boldsymbol{q} = 0$, black $:\Leftrightarrow \det \boldsymbol{q} = 1$. b) Cartesian illustration.

$\det \boldsymbol{q}$. However, the interpretation of Fig. 3b is not trivial. For a better understanding of material bifurcation, we use a different visualization technique. In the context of microplane theory, this visualization technique has been applied in [45]. The resulting spherical plot is shown in Fig. 3a. In this diagram, the value $\det \boldsymbol{q}/\det \boldsymbol{q}^{\text{el}}$ is indicated by means of different greyscales projected onto the unit sphere $\mathcal{S}^2$. White denotes $\det \boldsymbol{q}/\det \boldsymbol{q}^{\text{el}} = 1$ and black denotes $\det \boldsymbol{q}/\det \boldsymbol{q}^{\text{el}} = 0$, respectively. Consequently, critical bifurcation directions are associated with black color. The corresponding position vector $\boldsymbol{X}_P$ of the point $P \in \mathcal{S}^2$ is identical to the vector $\boldsymbol{n}$. Using Fig. 3a, the interpretation of the failure mode is trivial. According to the considered stress space, possible slip lines are located in a cone around the X_3-axis.

The second load case is characterized by the stress state

$$\boldsymbol{\sigma} = \sigma\,\boldsymbol{e}_1 \otimes \boldsymbol{e}_1 - \sigma\,\boldsymbol{e}_3 \otimes \boldsymbol{e}_3, \quad \text{with} \quad \sigma > 0. \tag{80}$$

According to [44], the ratio between the softening modulus and the YOUNG's modulus is assumed as $H/E = 0.0139$. The other material parameters are unchanged. The determinant of the acoustic tensor is illustrated in Fig. 4. Analogously to the first load case, the spherical

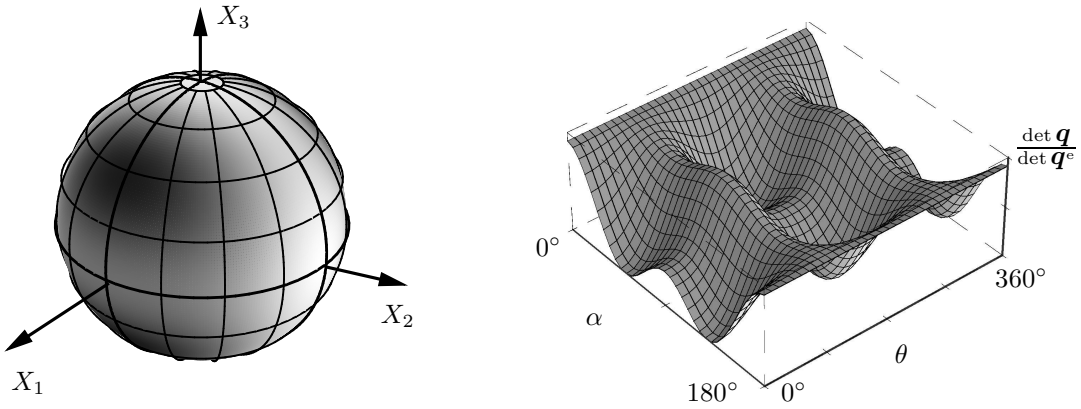

a) b)

Figure 4: Numerical bifurcation analysis: Determinant of the acoustic tensor (normalized): DRUCKER-PRAGER type plasticity model (see Table 3); stress state $\boldsymbol{\sigma} = \sigma\ \boldsymbol{e}_1 \otimes \boldsymbol{e}_1 - \sigma\ \boldsymbol{e}_3 \otimes \boldsymbol{e}_3$; $\nu = 0.2$: a) Spherical illustration (white $:\Leftrightarrow \det \boldsymbol{q} = 0$, black $:\Leftrightarrow \det \boldsymbol{q} = 1$. b) Cartesian illustration.

illustration is more proper.

Both load cases have been analyzed for different values of POISSON's ratio ν. For a comparison of the computed results with the analytically determined solutions in [44] an angle α_{crit} is introduced. α_{crit} is defined as

$$\alpha_{\text{crit}} := \min[\arccos[\boldsymbol{e}_3 \cdot \boldsymbol{n}] \pm 90°]. \tag{81}$$

The numerically obtained results are summarized in Table 4. They are identical to those re-

Load case	principal stresses			α_{crit}		
	σ_1	σ_2	σ_3	$\nu = 0.0$	$\nu = 0.2$	$\nu = 0.499$
Uniaxial compression	0.0	0.0	-2.0	48.19°	43.09°	35.29°
Shear	0.77	0.0	-0.77	39.45°	38.32°	36.62°

Table 4: Numerical bifurcation analyses: Computed angle α_{crit}. Principal stresses σ_1, σ_2 and σ_3 $f_{\text{c}} = 2.0$, $f_{\text{tu}} = 1.0$, plastic potential: VON MISES type ($\alpha_2 = 0$).

ported in [44]. To demonstrate the performance of the algorithm, the convergence of the local NEWTON iteration is shown in Table 5. As expected, an asymptotic quadratical convergence can be observed.

7 UNIQUENESS OF THE SOLUTION

In Section 5, an algorithmic formulation for the analysis of material bifurcation has been proposed. However, in general, the solution concerned with $\min \det \boldsymbol{q}$ is not unique. With the exception of RANKINE criterion based models, at least two different solutions exist. In the case

Iteration i	$\|\|\boldsymbol{\Delta}_i\|\|_\infty$
1	0.2879252280E-01
2	0.4627621106E-03
3	0.1519820538E-06
4	0.1674621005E-13

Table 5: Numerical bifurcation analysis: Convergence for load case „shear", $\nu = 0.2$, Initial value $\alpha_0 = 130°$, $\theta_0 = 0°$.

of uniaxial compression applied to a DRUCKER PRAGER type model (see Fig. 3), an infinite number of solutions exists. Consequently, it is convenient to introduce the set of all candidates

$$\mathbb{J}_{\boldsymbol{n}} := \left\{ \boldsymbol{n} \in \mathcal{S}^2 \mid \det \boldsymbol{q}(\boldsymbol{n}) \leq \det \boldsymbol{q}(\boldsymbol{n}^*),\ \forall \boldsymbol{n}^* \in \mathcal{S}^2 \right\}. \tag{82}$$

However, neglecting load cases which are invariant with respect to a rotation applied to special axes such as uniaxial stress states or hydrostatic stress states, not any element of $\mathbb{J}_{\boldsymbol{n}}$ has a physical relevance (see [46, 47]). Hence, the „right" bifurcation mode has to be chosen from $\mathbb{J}_{\boldsymbol{n}}$. For that purpose, different solution strategies have been developed. In [10, 27, 47], the vector $\boldsymbol{n}$ which results in a failure mode more closely aligned with the smooth deformation field $\bar{\boldsymbol{u}}$ is chosen. Locally, this idea can be rewritten into the format (at the onset of bifurcation $\boldsymbol{F} = \bar{\boldsymbol{F}}$, see Eq. (35))

$$\boldsymbol{N} = \arg\max_{\tilde{\boldsymbol{N}}} [\boldsymbol{F} : (\boldsymbol{m} \otimes \tilde{\boldsymbol{N}})], \quad \tilde{\boldsymbol{N}} = \tilde{\boldsymbol{n}} \cdot \boldsymbol{F}, \quad \tilde{\boldsymbol{n}} \in \mathbb{J}_{\boldsymbol{n}}. \tag{83}$$

Alternatively, in [48] the criterion

$$\boldsymbol{n} = \arg\max_{\tilde{\boldsymbol{n}}} \dot{\zeta}(\tilde{\boldsymbol{n}}) \qquad \tilde{\boldsymbol{n}} \in \mathbb{J}_{\boldsymbol{n}} \tag{84}$$

has been applied. Since ζ is associated with inelastic deformations, the vector $\boldsymbol{n}$ maximizing the inelastic deformations is chosen.

In what follows, we will first show that Eq. (84) is equivalent to the condition of maximum dissipation $\mathcal{D}$

$$\boldsymbol{n} = \arg\max_{\tilde{\boldsymbol{n}}} \mathcal{D}(\tilde{\boldsymbol{n}}) \qquad \tilde{\boldsymbol{n}} \in \mathbb{J}_{\boldsymbol{n}}. \tag{85}$$

Assuming isotropic softening behavior, the potential of a continuum with localized inelastic deformations at $\partial_{\mathrm{s}}\Omega$ and discontinuous displacement field results in

$$\Psi(\bar{\boldsymbol{C}}, \zeta) = \Psi_{\mathrm{e}}(\bar{\boldsymbol{C}}) + \delta_{\mathrm{s}}\ \Psi_{\mathrm{in}}(\zeta), \quad \text{with} \quad \bar{\boldsymbol{C}} := \bar{\boldsymbol{F}}^T \cdot \bar{\boldsymbol{F}}. \tag{86}$$

In Eq. (86), $\Psi_{\mathrm{e}}(\bar{\boldsymbol{C}})$ denotes the elastic stored energy potential and Ψ_{in} represents the potential function for a stress-like internal variable. Consequently, material points which belong to $\Omega^{\pm}$ unload elastically. For further details, we refer to [17, 28]. Using Eq. (86), the reduced dissipation is obtained as

$$\mathcal{D} = \boldsymbol{T} \cdot [\![\dot{\boldsymbol{u}}]\!]\ \delta_{\mathrm{s}} + q\ \dot{\zeta}\ \delta_{\mathrm{s}} \geq 0, \qquad q := -\partial_{\zeta}\Psi \tag{87}$$

or alternatively

$$\mathcal{D} = [\boldsymbol{T} \cdot \boldsymbol{m} + q]\ \dot{\zeta}\ \delta_{\mathrm{s}} \geq 0. \tag{88}$$

Similarly to standard continuum mechanics, the space of admissible stresses is defined

$$\mathbb{E}_{\boldsymbol{T}} := \left\{ (\boldsymbol{T}, q(\zeta)) \in \mathbb{R}^3 \times \mathbb{R}^+ \mid \phi(\boldsymbol{T}, q) \leq 0 \right\}. \tag{89}$$

In contrast to standard continuum mechanics, this space is defined in terms of the traction vector $\boldsymbol{T}$ acting on $\partial_{\mathrm{s}}\Omega$ and the stress-like variable q. Restricting our considerations to isotropic softening, the yield function ϕ is assumed as

$$\phi = \boldsymbol{T} \cdot \boldsymbol{m} - \sigma_{\mathrm{eq}}^{\mathrm{ini}} + q(\zeta) \leq 0, \tag{90}$$

i.e. an associative model is adopted (compare Eq. (90) with (87) and (88), respectively). From Eq. (90), the dissipation (88) simplifies to

$$\mathcal{D} = \sigma_{\mathrm{eq}}^{\mathrm{ini}} \, \dot{\zeta} \, \delta_{\mathrm{s}}. \tag{91}$$

Eq. (91) is similar to its counterpart in standard plasticity. In the presented framework, the amplitude of the displacement jump plays the role of the plastic multiplier. Applying Eq. (91), the equivalence

$$\dot{\zeta}(\boldsymbol{n}) \geq \dot{\zeta}(\tilde{\boldsymbol{n}}) \quad \Leftrightarrow \quad \mathcal{D}(\boldsymbol{n}) \geq \mathcal{D}(\tilde{\boldsymbol{n}}) \quad \forall \tilde{\boldsymbol{n}} \in \mathbb{J}_{\boldsymbol{n}}. \tag{92}$$

follows directly.

The proven equivalence holds also for kinematic softening. For that purpose, the yield function

$$\phi(\boldsymbol{T}, \boldsymbol{\xi}) = T_{\mathrm{eq}}(\boldsymbol{T} - \boldsymbol{\xi}) - \sigma_{\mathrm{eq}}^{\mathrm{ini}}, \quad \text{with} \quad \boldsymbol{\xi} = \partial_{[\![\boldsymbol{u}]\!]} \Psi_{\mathrm{in}}, \quad \Psi_{\mathrm{in}} = \Psi_{\mathrm{in}}([\![\boldsymbol{u}]\!]) \tag{93}$$

is considered. Assuming associative evolution equations ($\boldsymbol{m} = \partial_{\boldsymbol{T}} T_{\mathrm{eq}}$), the dissipation results in (see Eq. (88))

$$\mathcal{D} = [\boldsymbol{T} - \boldsymbol{\xi}] \cdot \partial_{\boldsymbol{T}} T_{\mathrm{eq}} \, \dot{\zeta} \, \delta_{\mathrm{s}} \geq 0. \tag{94}$$

According to many standard plasticity models, we make the additional assumption $T_{\mathrm{eq}}(\boldsymbol{A}) = \partial_{\boldsymbol{T}} T_{\mathrm{eq}} \cdot \boldsymbol{A}$, i.e. T_{eq} is a positively homogeneous function of degree one. From this, Eq. (94) reduces to

$$\mathcal{D} = \sigma_{\mathrm{eq}}^{\mathrm{ini}} \, \dot{\zeta} \, \delta_{\mathrm{s}} \geq 0. \tag{95}$$

Consequently, the equivalence (92) holds also for kinematic softening.

Next, we want to show the equivalence between the criterion (83) and (85). For that purpose, we use the equivalence (92) and compute the rate of the amplitude of the displacement jump. Using the consistency condition $\dot{\phi} = 0$ together with Eq. (90) this rate is obtained as

$$\dot{\phi} = 0 \quad \Rightarrow \quad \dot{\zeta} = H^{-1} \, (\boldsymbol{m} \otimes \boldsymbol{N}) : \dot{\boldsymbol{P}}, \quad \text{with} \quad H := -\partial_{\zeta} q. \tag{96}$$

Hence, the equivalence

$$\dot{\zeta}(\boldsymbol{n}) \geq \dot{\zeta}(\tilde{\boldsymbol{n}}) \quad \Leftrightarrow \quad (\boldsymbol{m} \otimes \boldsymbol{N}) : \dot{\boldsymbol{P}} \geq \left(\tilde{\boldsymbol{m}} \otimes \tilde{\boldsymbol{N}}\right) : \dot{\boldsymbol{P}} \tag{97}$$

holds (softening implies $H^{-1} > 0$). Consequently,

$$\begin{aligned} & (\boldsymbol{m} \otimes \boldsymbol{N}) : \dot{\boldsymbol{P}} \geq \left(\tilde{\boldsymbol{m}} \otimes \tilde{\boldsymbol{N}}\right) : \dot{\boldsymbol{P}} \\ \overset{!}{\Longleftrightarrow} \quad & (\boldsymbol{m} \otimes \boldsymbol{N}) : \boldsymbol{F} \geq \left(\tilde{\boldsymbol{m}} \otimes \tilde{\boldsymbol{N}}\right) : \boldsymbol{F}. \end{aligned} \tag{98}$$

However, the identity of criterion (83) and (85) cannot be proven on the basis of Ineq. (98). For the proof, we start with the discrete counterpart of the consistency condition $\phi_{n+1} := \phi(t_{n+1}) = 0$. Since the presented proof is restricted to isotropic material models, it is convenient to formulate the constitutive equations in the deformed configuration. Hence, the failure surface (90) is pushed forward leading to

$$\phi = \boldsymbol{\tau} : (\boldsymbol{m} \otimes \boldsymbol{n}) - \sigma_{\mathrm{eq}}^{\mathrm{ini}} + q(\zeta). \tag{99}$$

From the discrete consistency condition, the increment of the amplitude of the displacement jump (first corrector-step) is computed as

$$\Delta\zeta_{n+1} = H^{-1} \left[\boldsymbol{\tau}_{n+1} : (\boldsymbol{m} \otimes \boldsymbol{n}) - \sigma_{\text{eq}}^{\text{ini}}\right]. \tag{100}$$

Therefore, in the context of computational inelasticity, we have to show

$$\begin{aligned} & \boldsymbol{\tau}_{n+1} : (\boldsymbol{m} \otimes \boldsymbol{n}) \geq \boldsymbol{\tau}_{n+1} : (\tilde{\boldsymbol{m}} \otimes \tilde{\boldsymbol{n}}) \\ \overset{!}{\Longleftrightarrow} \quad & (\boldsymbol{m} \otimes \boldsymbol{N}) : \boldsymbol{F}_{n+1} \geq \left(\tilde{\boldsymbol{m}} \otimes \tilde{\boldsymbol{N}}\right) : \boldsymbol{F}_{n+1}. \end{aligned} \tag{101}$$

According to standard arguments of continuum mechanics, the second PIOLA-KIRCHHOFF stresses are obtained from the dissipation inequality as

$$\boldsymbol{S} = 2\, \partial_{\bar{\boldsymbol{C}}} \Psi. \tag{102}$$

In what follows, attention is restricted to isotropic potentials Ψ. Consequently, Ψ depends on $\bar{\boldsymbol{C}}$ via its invariants, which are equivalent to the invariants of $\bar{\boldsymbol{b}} := \bar{\boldsymbol{F}} \cdot \bar{\boldsymbol{F}}^T$, resulting in (see [26])

$$\boldsymbol{\tau} = 2\, \partial_{\bar{\boldsymbol{b}}} \Psi \cdot \bar{\boldsymbol{b}}. \tag{103}$$

With the three invariants $I_{\bar{\boldsymbol{b}}}$, $II_{\bar{\boldsymbol{b}}}$ and $III_{\bar{\boldsymbol{b}}}$ of $\bar{\boldsymbol{b}}$, Eq. (103) can be rewritten into the format

$$\boldsymbol{\tau} = 2\, \frac{\partial \psi}{\partial \boldsymbol{b}} \cdot \boldsymbol{b} = 2 \left[\frac{\partial \psi}{\partial III_{\boldsymbol{b}}}\right] \boldsymbol{1} + 2 \left[\frac{\partial \psi}{\partial I_{\boldsymbol{b}}} + \frac{\partial \psi}{\partial II_{\boldsymbol{b}}}\, I_{\boldsymbol{b}}\right] \boldsymbol{b} - 2\, \frac{\partial \psi}{\partial II_{\boldsymbol{b}}}\, \boldsymbol{b}^2. \tag{104}$$

Since the stresses $\boldsymbol{\tau}$ depend on $\bar{\boldsymbol{b}}$, it is necessary to reformulate the inequality $(101)_2$ in terms of $\bar{\boldsymbol{b}}$. Applying the transformation $\boldsymbol{N} = \boldsymbol{n} \cdot \bar{\boldsymbol{F}}$, we obtain

$$\boldsymbol{F} : (\boldsymbol{m} \otimes \boldsymbol{N}) = \left(\bar{\boldsymbol{F}} \cdot \bar{\boldsymbol{F}}^T\right) : (\boldsymbol{n} \otimes \boldsymbol{m}) = \bar{\boldsymbol{b}} : (\boldsymbol{n} \otimes \boldsymbol{m}). \tag{105}$$

To prove the equivalence (101), we first show the implication "$\Longleftarrow$". For that purpose, two different candidates $\boldsymbol{n}, \tilde{\boldsymbol{n}} \in \mathbb{J}_{\boldsymbol{n}}$ and their corresponding vectors $\boldsymbol{m}, \tilde{\boldsymbol{m}}$ characterized by

$$\bar{\boldsymbol{b}} \cdot (\boldsymbol{m} \otimes \boldsymbol{n}) \geq \bar{\boldsymbol{b}} \cdot (\tilde{\boldsymbol{m}} \otimes \tilde{\boldsymbol{n}}) \tag{106}$$

are considered. Double contraction of $\boldsymbol{m} \otimes \boldsymbol{n}$ with the stress tensor yields

$$\begin{aligned} \boldsymbol{\tau} : (\boldsymbol{m} \otimes \boldsymbol{n}) \;=\; & 2 \left[\frac{\partial \psi}{\partial III_{\boldsymbol{b}}}\right] (\boldsymbol{m} \cdot \boldsymbol{n}) \\ & + \; 2 \left[\frac{\partial \psi}{\partial I_{\boldsymbol{b}}} + \frac{\partial \psi}{\partial II_{\boldsymbol{b}}}\, I_{\boldsymbol{b}}\right] \boldsymbol{b} : (\boldsymbol{m} \otimes \boldsymbol{n}) \\ & - \; 2\, \frac{\partial \psi}{\partial II_{\boldsymbol{b}}}\, \boldsymbol{b}^2 : (\boldsymbol{m} \otimes \boldsymbol{n}). \end{aligned} \tag{107}$$

Next, we assume $\Psi = \Psi(I_{\bar{\boldsymbol{b}}}, III_{\bar{\boldsymbol{b}}})$. This restriction is fulfilled for many material. For instance, NEO-HOOKE type material models are characterized by this assumption (see [49, 50]). Neglecting the second invariant of $\bar{\boldsymbol{b}}$, Eq. (107) reduces to

$$\boldsymbol{\tau} : (\boldsymbol{m} \otimes \boldsymbol{n}) = 2 \left[\frac{\partial \psi}{\partial III_{\boldsymbol{b}}}\right] (\boldsymbol{m} \cdot \boldsymbol{n}) + 2 \left[\frac{\partial \psi}{\partial I_{\boldsymbol{b}}}\right] \boldsymbol{b} : (\boldsymbol{m} \otimes \boldsymbol{n}). \tag{108}$$

Using Ineq. (106), we obtain

$$\boldsymbol{\tau} : (\boldsymbol{m} \otimes \boldsymbol{n}) \geq 2 \left[\frac{\partial \psi}{\partial III_{\boldsymbol{b}}}\right] (\boldsymbol{m} \cdot \boldsymbol{n}) + 2 \left[\frac{\partial \psi}{\partial I_{\boldsymbol{b}}}\right] \boldsymbol{b} : (\tilde{\boldsymbol{m}} \otimes \tilde{\boldsymbol{n}}) \,. \tag{109}$$

In Ineq. (108) $\partial \Psi / \partial I_{\bar{\boldsymbol{b}}} \geq 0$ has been applied (see [49]). Since all vectors $\boldsymbol{n} \in \mathbb{J}_{\boldsymbol{n}}$ show the same localization mode characterized by the absolute value $|\boldsymbol{n} \cdot \boldsymbol{m}|$ ($|\boldsymbol{n} \cdot \boldsymbol{m}| = 1 \Leftrightarrow$ mode-I failure, $|\boldsymbol{n} \cdot \boldsymbol{m}| = 0 \Leftrightarrow$ mode-II failure and $|\boldsymbol{n} \cdot \boldsymbol{m}| \in (0,1) \Leftrightarrow$ mixed-mode failure), we assume without loss of generality

$$\boldsymbol{n} \cdot \boldsymbol{m} = \tilde{\boldsymbol{n}} \cdot \tilde{\boldsymbol{m}}. \tag{110}$$

Inserting the identity (110) into Ineq. (109) finishes the proof

$$\begin{aligned} \boldsymbol{\tau} : (\boldsymbol{m} \otimes \boldsymbol{n}) \geq \quad & 2 \left[\frac{\partial \psi}{\partial III_{\boldsymbol{b}}}\right] (\tilde{\boldsymbol{m}} \cdot \tilde{\boldsymbol{n}}) \\ + \quad & 2 \left[\frac{\partial \psi}{\partial I_{\boldsymbol{b}}}\right] \boldsymbol{b} : (\tilde{\boldsymbol{m}} \otimes \tilde{\boldsymbol{n}}) = \boldsymbol{\tau} : (\tilde{\boldsymbol{m}} \otimes \tilde{\boldsymbol{n}}) \,. \end{aligned} \tag{111}$$

The other implication of equivalence (101) can be proven similarly.

8 CONCLUSION

An algorithmic formulation for the analyses of discontinuous material bifurcation has been presented in this paper. For that purpose, first the conditions associated with the formation of weak and strong discontinuities have been described. In particular, the localization condition corresponding to the onset of discontinuous displacement fields was analyzed in detail and extended to anisotropic materials. Based on an unconstrained optimization problem formulated in terms of spherical coordinates, NEWTON's method has been applied for the computation of the resulting localization conditions. To obtain a globally convergent algorithm, a line search strategy has been adopted. The applicability of the proposed implementation as well as its performance and numerical robustness has been investigated by means of three-dimensional numerical bifurcation analyses of a non-associative DRUCKER-PRAGER type plasticity model.

However, in general, the solution of the localization condition is not unique. Consequently, the „right" bifurcation mode has to be chosen from a set containing all candidates. For that purpose, existing strategies have been reviewed and interpreted critically. The analogies between them have been pointed out.

Since the knowledge about the topology of singular surfaces is of major importance for numerical models based on discontinuous displacement fields such as the Strong Discontinuity Approach (SDA) (see [9, 18–20, 29]) as well as the X-Fem (see [51, 52]), the application range of the proposed implementation is very broad.

Acknowledgement

This work was completed under the financial support of the Deutsche Forschungsgemeinschaft (DFG) through project A4 under supervision of Prof. O.T. Bruhns within the Collaborative Research Centre 398. The author wishes to express his sincere gratitude to this support. Furthermore, the author would like to thank Prof. O.T. Bruhns for his helpful comments.

References

[1] A. Nádai. *Plasticity*. Mc Graw-Hill, New York - London, 1931.

[2] J. Hadamard. Leçons sur la Propagation des Ondes. *Librairie Scientifique A. Hermann et Fils, Paris*, 1903.

[3] J.W. Rudnicki and J.R. Rice. Conditions for localization of deformation in pressure-sensitive dilatant materials. *Journal of the Mechanics and Physics of Solids*, 23:371–394, 1975.

[4] J.R. Rice and J.W. Rudnicki. A note on some features of the theory of localization of deformation. *International Journal for Solids and Structures*, 16:597–605, 1980.

[5] B. Raniecki and O.T. Bruhns. Bounds to bifurcation stresses in solids with non-associated plastic flow law at finite strains. *Journal of the Mechanics and Physics of Solids*, 29(2):153–172, 1981.

[6] N.S. Ottosen and K. Runesson. Properties of discontinuous bifurcation solutions in elasto-plasticity. *International Journal for Solids and Structures*, 27(4):401–421, 1991.

[7] K. Runesson, N.S. Ottosen, and D. Perić. Discontinuous bifurcations of elastic-plastic solutions at plane stress and plane strain. *International Journal of Plasticity*, 7:99–121, 1991.

[8] E. Rizzi, I. Carol, and K. Willam. Localization analysis of elastic degradation with application to scalar damage. *Journal of Engineering Mechanics (ASCE)*, 121:541–554, 1995.

[9] J. Simo, J. Oliver, and F. Armero. An analysis of strong discontinuities induced by strain softening in rate-independent inelastic solids. *Computational Mechanics*, 12:277–296, 1993.

[10] F. Armero and K. Garikipati. An analysis of strong discontinuities in multiplicative finite strain plasticity and their relation with the numerical simulation of strain localization in solids. *International Journal for Solids and Structures*, 33:2863–2885, 1996.

[11] J. Oliver, M. Cervera, and O. Manzoli. Strong discontinuities and continuum plasticity models: The strong discontinuity approach. *International Journal of Plasticity*, 15:319–351, 3 1999.

[12] J. Oliver, A.E. Huespe, M.D.G. Pulido, and E. Samaniego. On the strong discontinuity approach in finite deformation settings. *International Journal for Numerical Methods in Engineering*, 56:1051–1082, 2003.

[13] M. Ortiz. An analytical study of the localized failure modes of concrete. *Mechanics of Materials*, 6:159–174, 1987.

[14] M. Ortiz, Y. Leroy, and A. Needleman. A finite element method for localized failure analysis. *Computer Methods in Applied Mechanics and Engineering*, 61:189–214, 1987.

[15] P. Papadopoulos and J. Li. A general framework for the numerical solution of problems in finite elasto-plasticity. *Computer Methods in Applied Mechanics and Engineering*, 159:1–18, 1998.

[16] P. Papadopoulos and J. Li. On the formulation and numerical solution of problems in anisotropic finite plasticity. *Computer Methods in Applied Mechanics and Engineering*, 190:4889–4910, 2001.

[17] J. Mosler. *Finite Elemente mit sprungstetigen Abbildungen des Verschiebungsfeldes für numerische Analysen lokalisierter Versagenszustände in Tragwerken*. PhD thesis, Ruhr University Bochum, 2002.

[18] J. Oliver. Modelling strong discontinuities in solid mechanics via strain softening constitutive equations part 1: Fundamentals. part 2: Numerical simulations. *International Journal for Numerical Methods in Engineering*, 39:3575–3623, 1996.

[19] M. Jirásek and T. Zimmermann. Embedded crack model: Part I: Basic formulation, Part II: Combination with smeared cracks. *International Journal for Numerical Methods in Engineering*, 50:1269–1305, 2001.

[20] J. Mosler and G. Meschke. 3D modeling of strong discontinuities in elastoplastic solids: Fixed and rotating localization formulations. *International Journal for Numerical Methods in Engineering*, 57:1553–1576, 2003.

[21] J.C. Maxwell. *Treatise on Electricity and Magnetism*. Clarendom, Oxford, 1873.

[22] I. Stakgold. *Boundary value problems of mathematical physics*, volume I. Macmillien Series in Advanced Mathematics and theoretical physics, 1967.

[23] I. Stakgold. *Boundary value problems of mathematical physics*, volume II. Macmillien Series in Advanced Mathematics and theoretical physics, 1967.

[24] I. Stakgold. *Green's functions and boundary value problems*. Wiley, 1998.

[25] J. Simo and T.J.R. Hughes. *Computational inelasticity*. Springer, New York, 1998.

[26] J.C. Simo. Numerical analysis of classical plasticity. In P.G. Ciarlet and J.J. Lions, editors, *Handbook for numerical analysis*, volume IV. Elsevier, Amsterdam, 1998.

[27] K. Garikipati. *On strong discontinuities in inelastic solids and their numerical simulation*. PhD thesis, Stanford University, 1996.

[28] F. Armero. Large-scale modeling of localized dissipative mechanisms in a local continuum: applications to the numerical simulation of strain localization in rate-dependent inelastic solids. *Mechanics of Cohesive-Frictional Materials*, 4:101–131, 1999.

[29] R.I. Borja. Finite element simulation of strain localization with large deformation: capturing strong discontinuity using a Petrov-Galerkin multiscale formulation. *Computer Methods in Applied Mechanics and Engineering*, 2002. in press.

[30] J. Mosler and G. Meschke. Embedded crack vs. smeared crack models: A comparison of elementwise discontinuous crack path approaches with emphasis on mesh bias. *Computer Methods in Applied Mechanics and Engineering*, 193:3351–3375, 2004.

[31] A.R. Regueiro and R.I. Borja. A finite element method of localized deformation in frictional materials taking a strong discontinuity approach. *Finite Elements in Analysis and Design*, 33:283–315, 1999.

[32] J. Mosler and Bruhns O.T. A 3D anisotropic elastoplastic-damage model using discontinuous displacement fields. *International Journal for Numerical Methods in Engineering*, 60:923–948, 2004.

[33] R.I. Borja. Bifurcation of elastoplastic solids to shear band mode at finite strains. *Computer Methods in Applied Mechanics and Engineering*, 191:5287–5314, 2002.

[34] P. Steinmann, R. Larsson, and K. Runesson. On the localization properties of multiplicative hyperelasto-plastic continua with strong discontinuities. *International Journal for Solids and Structures*, 34:969–990, 1997.

[35] A.E. Green and P.M. Naghdi. A general theory of an elastic-plastic continuum. *Arch. Rat. Mech. Anal.*, 18:251–281, 1965.

[36] J. Schröder, F. Gruttmann, and J. Löblein. A simple orthotropic finite elasto-plasticity model based on generalized stress-strain measures. *Computational Mechanics*, 30:48–64, 2002.

[37] C. Miehe, N. Apel, and M. Lambrecht. Anisotropic additive plasticity in the logarithmic strain space: modular kinematic formulation and implementation based on incremental minimization principles for standard materials. *Computer Methods in Applied Mechanics and Engineering*, 191:5383–5425, 2002.

[38] E.H. Lee. Elastic-plastic deformation at finite strains. *Journal of Applied Mechanics*, 36:1–6, 1969.

[39] O.T. Bruhns, H. Xia, and A. Meyers. A self-consistent Eulerian rate type model for finite deformation elastoplasticity with isotropic damage. *International Journal for Solids and Structures*, 38:657–683, 2001.

[40] D.G. Luenberger. *Linear and nonlinear programming*. Addison-Wesley Publishing Company, second edition, 1984.

[41] R. Fletcher. *Practical Methods of Optimization*. Wiley, New York, second edition, 1991.

[42] G.L. Nemhauser. *Handbooks in Operation Research and Management Science*, volume 1: Optimization. Elsevier, second edition, 1989.

[43] Kirsch. *Structural optimization*. Springer, Berlin, 1993.

[44] M.M. Iordache and K. Willam. Localized failure modes in cohesive-frictional materials. Technical report, Structural Engineering and Structural Mechanics research series, Department of civil, environmental & architectural engineering, University of Colorado at Boulder, 1996.

[45] D. Kuhl, S. Müller, and G. Meschke. An extension of the microplane model for the modeling of anisotropic elasticity and damage for particle based recycling materials. In *Trends in Computational Structural Mechanics*. CIMNE, Barcelona, 2001.

[46] J. Simo and J. Oliver. A new approach to the analysis and simulation of strain softening in solids. In Z.P. Bažant, Z. Bittnar, M. Jirásek, and J. Mazars, editors, *Fracture and Damage in Quasibrittle Structures*, pages 25–39. E. &F.N. Spon, London, 1994.

[47] R.I. Borja. A finite element model for strain localization analysis of strongly discontinuous fields based on standard galerkin approximation. *Computer Methods in Applied Mechanics and Engineering*, 190:1529–1549, 2000.

[48] G.N. Wells and L.J. Sluys. Analysis of slip planes in three-dimensional solids. *Computer Methods in Applied Mechanics and Engineering*, 190:3591–3606, 2001.

[49] P. Ciarlet. *Mathematical elasticity. Volume I: Three-dimensional elasticity*. North-Holland Publishing Company, Amsterdam, 1988.

[50] Y Başar and D. Weichert. *Nonlinear continuum mechanics of solids*. Springer, 2000.

[51] N. Moës, J. Dolbow, and T. Belytschko. A finite element method for crack growth without remeshing. *International Journal for Numerical Methods in Engineering*, 46:131–150, 1999.

[52] N. Sukumar, N. Moës, B. Moran, and T. Belytschko. Extended finite element method for three-dimensional crack modelling. *International Journal for Numerical Methods in Engineering*, 48:1549–1570, 2000.